DESIGN AND CONSTRUCTION OF A PERMANENT MAGNET SYNCHRONOUS MOTOR

MISS SISUDA CHAITHONGSUK

A THESIS SUBMITTED INPARTIAL FULFILLMENT OF THE REQUIREMENTS
FOR THE MASTER OF ENGINEERING IN ELECTRICAL ENGINEERING
DEPARTMENT OF ELECTRICAL ENGINEERING
GRADUATE COLLEGE
KING MONGKUT'S INSTITUTE OF TECHNOLOGY NORTH BANGKOK
ACADEMIC YEAR 2006
ISBN 974-190-887-3

Name : Miss Sisuda Chaithongsuk
Thesis Title : Design and Construction of a Permanent Magnet Synchronous Motor
Major Field : Electrical Engineering
King Mongkut's Institute of Technology North Bangkok
Thesis Advisors : Associate Professor Dr.Suksun Nungam
Assistant Professor Panarit Sethakul
Academic Year : 2006

Abstract

Permanent Magnet Synchronous Motors(PMSMs) have been widely used in many industrial applications. This thesis presents the design and construction of a permanent magnet synchronous motor. The permanent magnet rotor was constructed based on the stator frame of a three-phase induction motor. The design is performed in order to achieve a sinusoidal back EMF without changing the stator geometry and winding. Each pole of the rotor is fixed with several magnet blocks. The main difficulty is to choose the appropriate elementary magnet block span. Therefore, the optimum value of magnet span is chosen to minimize the THD of back EMF. Torque and cogging torque are considered in the design. The finite element method is used in the design calculation. The experimental results are compared with the calculation results.

(Total 68 pages)

Keywords : Magnet span, Permanent magnet synchronous motor and Cogging torque

_____ Advisor

ชื่อ : นางสาวศรีสุดา ไชยทองสุก
ชื่อวิทยานิพนธ์ : การออกแบบและสร้างมอเตอร์ซิงโครนัสชนิดแม่เหล็กถาวร
สาขาวิชา : วิศวกรรมไฟฟ้า
สถาบันเทคโนโลยีพระจอมเกล้าพระนครเหนือ
ที่ปรึกษาวิทยานิพนธ์ : รองศาสตราจารย์ ดร.สุขสันติ์ นุ่นงาม
ผู้ช่วยศาสตราจารย์ พนาฤทธิ์ เศรษฐกุล
ปีการศึกษา : 2549

บทคัดย่อ

ปัจจุบันมอเตอร์ซิงโครนัสชนิดแม่เหล็กถาวรมีการประยุกต์และใช้งานกันอย่างแพร่หลายในภาคอุตสาหกรรม งานวิจัยนี้ได้นำเสนอถึงการออกแบบและสร้างมอเตอร์ซิงโครนัสชนิดแม่เหล็กถาวร โดยการใช้โครงสร้างในส่วนของสเตเตอร์ที่มีอยู่เดิมของมอเตอร์เหนี่ยวนำ 3 เฟส และจะไม่มีการเปลี่ยนแปลงลักษณะรูปร่างของสเตเตอร์และขดลวดตัวนำ ซึ่งการออกแบบนี้เพื่อที่จะทำให้ได้แรงดัน Back-emf มีลักษณะเป็นรูปคลื่นไซน์ โดยในแต่ละขั้วจะมีแม่เหล็กถาวรหลายๆแท่งติดอยู่บนตัวโรเตอร์ สิ่งที่ยากที่สุดในการออกแบบคือ การเลือกขนาดมุมของแม่เหล็กที่เหมาะสม เพราะฉะนั้นค่าของมุมที่เหมาะสมจะทำให้ได้ผลรวมความผิดเพี้ยนของฮาร์มอนิกส์ (THD)ที่แรงดัน Back-emf มีค่าต่ำ ในขณะที่แรงบิด(Torque) และค่า Cogging torque ก็ถูกนำมาใช้ในการออกแบบด้วย โดยการคำนวณจะใช้วิธีการของ Finite Element Magnetic Method : FEMM และผลลัพธ์ที่ได้จากการทดลองจริงได้ถูกนำมาเปรียบเทียบกับการออกแบบที่ได้จากการคำนวณ

(วิทยานิพนธ์มีจำนวนทั้งสิ้น 68 หน้า)

คำสำคัญ : Magnet span, Permanent magnet synchronous motor และ Cogging torque

_____อาจารย์ที่ปรึกษาวิทยานิพนธ์

ACKNOWLEDGEMENTS

First of all, I am gratified with the kindness of Dr.Noureddine Takorabet for his guidance and I would like to express in French “Les remerciements les plus sincères sont dédiés à Professeur Dr.Noureddine Takorabet pour son attention et sa détermination de me transférer son savoir-faire ce qui ne m'était pas évident. Pourtant il est finalement la force motrice de cette réussite. Je vais appliquer tout son savoir-faire transféré et prendre professeur comme exemplaire pour mon travail dans la future ainsi que pour mon pays si l'occasion me présente”.

Next, I am grateful to Associate Professor Dr.Suksun Nungam who always support and suggest me in everything and also especially, Assistant Professor Panarit Sethakul, Director of Thai-French Innovation Centre, who gives me the great occasion in my life to learn the others technologies including the subsistence of the human. At last, I would like to thank all staffs of TFIC for their assistance.

Special thanks to my family and friends for the cares and supports me.

Sisuda Chaithongsuk

TABLE OF CONTENTS

LIST OF TABLES

LIST OF FIGURES

LIST OF FIGURES (CONTINUED)

LIST OF ABBREVIATIONS AND SYMBOLS

A	Area	[m^2]
a	Thickness magnet	[mm]
B	Magnetic flux density	[T]
$\hat{B}_{g(1)}$	Fundamental total flux density amplitude in air-gap	[T]
B_{mg}	Flux density in air-gap over magnet	[T]
$\hat{B}_{mg(1)}$	Fundamental magnet flux density amplitude in air-gap	[T]
B_r	Remanence flux density	[T]
e	Air-gap	[mm]
H	Magnetic field strength	[A/m]
H_c	Coercive force	[A/m]
I	Current	[A]
J	Current density	[A/m^2]
L	Inductance	[H]
M	Mutual inductance	[H]
N	Number of turn	[turns]
p	Number of pole	
q	Number of slot per pole and phase	
R_a	Internal radius of the stator	[mm]
R_r	Rotor radius	[mm]
φ	Magnetic flux	[Vs]
φ_1	Magnetic flux at circuit 1	[Vs]
φ_{12}	Magnetic flux at circuit 1 and circuit 2	[Vs]
λ	Flux linkage	
α	Magnet angle	[rad,°]
μ	Permeability	[$VsA^{-1}m^{-1}$]
μ_0	Permeability of free space	[$VsA^{-1}m^{-1}$]
	$\mu_0 = 4\pi\times10^{-7}$ $VsA^{-1}m^{-1}$	
μ_r	relative permeability	
ρ	Resistivity of the copper	[ohm.m]
cos(φ)	Power factor	

CHAPTER 1
INTRODUCTION

1.1 Motivation

Currently AC motors are favorably used in many industrial applications. Squirrel cage induction motors are particularly popular because of their simple structure, low cost production and less maintenance. However, the limitation of the induction motors is the working speed which is lower than the speed of rotating magnetic field and the changing slip depends on load torque. That is, an increasing in load torque results in the decreasing in working speed. Hence, the induction motors are not suitable for applications which require an accurate control of speed and position such as servo systems. On the other hand, speed of synchronous motors can be accurately controlled by varying the frequency of the rotating magnetic field which is called synchronous speed. However, the synchronous motors suffer from high production and maintenance costs.

Permanent magnet synchronous motors (PMSMs) have been widely used in many industrial applications. Due to their compactness and high torque density [1], the PMSMs are particularly used in high-performance drive systems such as the submarine propulsion. The permanent magnet synchronous motor eliminates the use of slip rings for field excitation, resulting in low maintenance and low losses in the rotor. The PMSMs have the high efficiency and are appropriate for high performance drive systems such as CNC machines, robotic and automatic production systems in the industry.

Generally, the design and construction a PMSM must consider both of the stator and rotor structures in order to obtain a high performance motor. However this thesis focuses only on the design of the permanent magnet rotor and uses the stator structure from an existing induction motor without changing the windings. That is, the squirrel cage rotor is replaced by a newly designed permanent magnet rotor.

In the design of the permanent magnet rotor, it is important to determine the optimum value of “magnet span” because it effects the harmonics of the back-emf and the cogging torque. The design is based on the finite element analysis using the software called Finite Element Magnetic Method or FEMM. The rotor is constructed using the optimum magnet span obtained from the computation by FEMM. The experimental results are compared with the results from the calculation.

This thesis is carried out as a part of the technical cooperation between Institut National Polytechnique de Lorraine (INPL), FRANCE and King Mongkut Institute of Technology North Bangkok, THAILAND. One of the objectives of this cooperation is to develop technical knowhow on electric motor designs for the industry in our country.

1.2 Thesis objectives

1.2.1 To apply the finite element analysis in the PMSM design.

1.2.2 To construct the permanent magnet rotor.

1.2.3 To compare the experimental results with the calculation results.

1.3 Thesis boundaries

The scope of the thesis includes the design and construction of a permanent magnet rotor based on the stator frame of a three-phase 1-Hp induction motor. Each pole of the rotor is fixed with several magnet blocks. The optimum magnet span is chosen to minimize the THD of back EMF of the motor. A finite element method is used in the design calculation. Torque and cogging torque are considered in the design.

1.4 Thesis procedure

1.4.1 Study research works regarding the design of PMSMs.
1.4.2 Study the fundamental of 3 phase induction motor and synchronous motor.
1.4.3 Study the fundamental of electromagnetic field.
1.4.4 Study the application of finite element method in motor design.
1.4.5 Test and find the parameters of the induction motor whose the stator frame is used in the design.
1.4.6 Study the program for designing by finite element magnetic method: FEMM.
1.4.7 Compute and design the permanent magnet for the rotor.
1.4.8 Construct the rotor.
1.4.9 Assemble the rotor to the stator and experiment.
1.4.10 Conclude the results.

1.5 Expected benefits

1.5.1 Obtain the method to design the permanent magnet synchronous motor.
1.5.2 Encourage the corresponding objective research.
1.5.3 Obtain the way to develop the high performance motor in the industry.
1.5.4 Support the potentiality for technology development in our country.

CHAPTER 2
BASIC IN ELECTROMAGNETIC AND NUMERICAL METHODS

The engineers or the sciences need to know the physic of electromagnetic field that it permeates through all space. Electromagnetic filed comprises of electric field and magnetic field. The electric field is produced by non-moving charges and the magnetic field is produced by moving charges(currents) and depicts as the source of the field. The way in which charges and currents interact with the electromagnetic field is described by Maxwell's equations and Lorentz Force Law [2].

The principle of electromagnetic and magnetostatics are used for designing the permanent magnet synchronous motor in this thesis. Finite element methods are used for the numerical computation of Maxwell's equations.

2.1 BIOT – SAVART'S LAW

Following the Biot – Savart's law, the mathematical relation between the magnetic field intensity and the current which produces the filed is as follows [3]

$$dH_2 = \frac{I_1 dL_1 \times a_{12}}{4\pi R_{12}^2} \qquad \text{Eq. 2-1}$$

where Figure 2-1 identifies each term in the equation. Subscripts are included in this introduction to the Biot – Savart law to clarify the location of each element. Equation 2-1 is analogous to the Coulomb's law equation for the electric field resulting from a differential charge,

$$dE_2 = \frac{dQ_1 a_{12}}{4\pi\varepsilon R_{12}^2} \qquad \text{Eq. 2-2}$$

To get the total field resulting from a current can be found by integrating the contributions from each segment by,

$$H = \int \frac{IdL \times aR}{4\pi R^2} \qquad \text{Eq. 2-3}$$

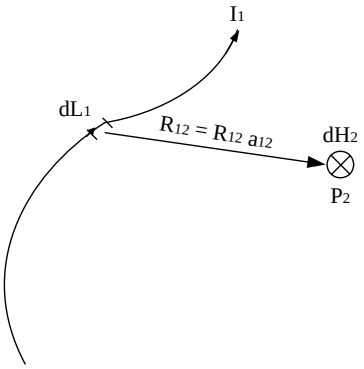

FIGURE 2-1 Illustration of the law of Biot-Savart showing magnetic field arising from a differential segment of current

Progression from Equation 2-1 to 2-3 is possible because, just like electric fields, they can be added by superposition.

2.2 AMPERE'S CIRCUITAL LAW

In electrostatic problems that feature considerable symmetry, it is easier to apply Gauss's law to solve for the electric field intensity than using the Coulomb's law. Likewise, in magnetostatic problems with sufficient symmetry, Ampère's circuital law can be applied more easily than the law of Biot-Savart.

$$\oiint_S D \cdot ds = Q \qquad (\textit{Gauss's law}\text{–int}\textit{egral form}) \qquad \text{Eq. 2-4}$$

Ampère's circuital law says that the integration of H around any closed path is equal to the net current enclosed by that path. This is state in equation form as

$$\oint H \cdot dL = I_{enc} \qquad (\textit{Ampère's law}\text{–int}\textit{egral form}) \qquad \text{Eq. 2-5}$$

The line integral of H around a closed path is termed the circulation of H. The path of the circulation does not matter in solving for the current enclosed, but in practical application, a symmetrical current distribution is given and you want to solve for H, so it is important to make a careful selection of an Amperian path (analogous to a Gaussian surface) that is everywhere either tangential or normal to H, and over which H is constant.

The direction of the circulation is chosen such that the right-hand rule is satisfied. That is, with the thumb in the direction of the current, the fingers will curl in the direction of the circulation.

Example : Infinite-length line current

Given a infinite-length line current I lying along the z-axis, use Ampère's law to determine the magnetic field by integrating the magnetic field around a circular path of radius ρ lying in the $x-y$ plane.

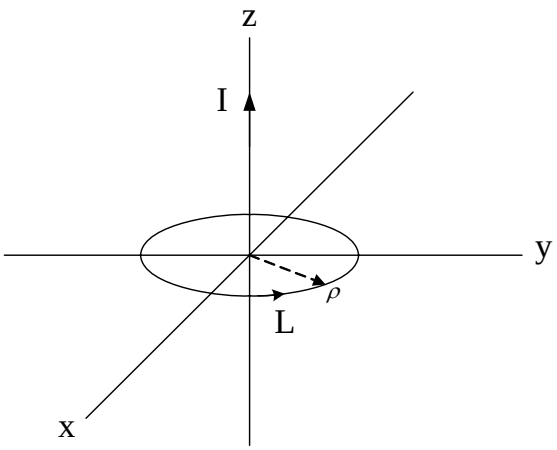

FIGURE 2-2 Amperian path around an infinite length of current

From Ampère's law,

$$\oint_L H \cdot dl = \oint_L H\varphi \cdot dl = I \qquad \text{Eq. 2-6}$$

by symmetry, the magnetic field is uniform on the given path so that

$$H\varphi \oint_L dl = H\varphi 2\pi\rho = I \qquad \text{Eq. 2-7}$$

or

$$H\varphi = \frac{I}{2\pi\rho} \qquad \text{Eq. 2-8}$$

2.3 Maxwell's equations

All four Maxwell's equations for static fields have been defined in both integral form and differential form. Maxwell's equations for time varying fields contain additional terms which form a compete set of coupled equations (all four equations must be satisfied simultaneously). Four Maxwell's equations are de-coupled into two sets of two equations : two for electrostatic field and two for magnetostatic fields.

Maxwell's equations for static fields are:

Integral form	Differential form	
$\oint_S D \cdot ds = \iiint_v \rho_v \, dv = Q_{enclosed}$	$\nabla \cdot D = \rho_v$	Eq. 2-9
$\oint_L E \cdot dl = 0$	$\nabla \times E = 0$	Eq. 2-10
$\oint_S B \cdot ds = 0$	$\nabla \cdot B = 0$	Eq. 2-11
$\int_L H \cdot dl = \iint_S J \cdot ds = I_{enclosed}$	$\nabla \times H = J$	Eq. 2-12

Equation 2-9 is called Gauss's law (electric fields).
Equation 2-10 is called Faraday's law.
Equation 2-11 is called Gauss's law (magnetic fields).
Equation 2-12 is called Ampère's law.

The differential, or point, form of Maxwell's equations are easily derived by applying the divergence theorem and Stoke's theorem to the integral form of the equations.

2.3.1 Differential operators in electromagnetic

The differential form of governing equations in electromagnetic (Maxwell's equations and related equations) are defined in terms of four different differential operators: the gradient operator, the divergence operator, the Laplacian operator. All of these operators can be defined in terms of the gradient (nabla ∇) operator.
Operators involving ∇:

Operator	Example	Operand	Result
Gradient	$\nabla V = -E$	scalar	Vector
Divergence	$\nabla \cdot D = \rho_v$	vector	Scalar
Laplacian	$\nabla^2 V = \frac{-\rho_v}{\varepsilon}$	scalar	Scalar
Curl	$\nabla \times H = J$	vector	Vector

Note that the two operators that operate on vectors (divergence and curl) are the two operators found in the differential form of Maxwell's equations. Certain characteristics of the vector fields in Maxwell's equations can be determined based on the divergence and curl results for these fields.

Characteristics of F based on $\nabla \cdot F$

Vectors with nonzero divergence $(\nabla \cdot F \neq 0)$ vary in the direction of the field.

Vectors with zero divergence $(\nabla \cdot F = 0)$ do not vary in the direction of the field.

The divergence of a vector F at a point P can be visualized by enclosing the point by an infinitesimally small differential volume and examining flux vector in and out of the volume. If there is a net flux out of the volume (more flux out of the volume than into the volume), the divergence of F is positive at the point P. If there is a net flux into the volume (more flux into the volume than out the volume), the divergence of F is negative at the point P.

$(\nabla \cdot F)_p > 0$

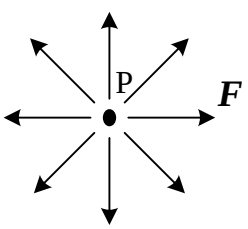

$(\nabla \cdot F)_p < 0$

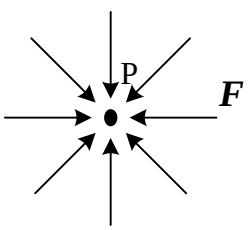

If the net flux into the differential volume is zero (the flux into the volume equals the flux out of the volume), the divergence of F is zero at the point P.

$$(\nabla \cdot F)_P = 0$$

According to Gauss's law for electric fields in differential form,

$$\nabla \cdot D = \rho_v \qquad \text{Eq. 2-13}$$

the divergence of the electric flux density is zero in a charge free region $(\rho_v = 0)$ and non zero in a region where charge is present. Thus, the divergence of the electric flux density locates the source of the electrostatic field (net positive charge = net flux out and net negative charge = net flux in).

According to Gauss's law for magnetic fields in differential form,

$$\nabla \cdot B = 0 \qquad \text{Eq. 2-14}$$

the divergence of the magnetic flux density is always zero since there is no magnetic charge (net flux = 0).

Characteristics of F based on $\nabla \times F$

Vectors with nonzero curl ($\nabla \times F \neq 0$) vary in a direction perpendicular to the direction of the field.

Vectors with zero curl ($\nabla \times F = 0$) do not vary in a direction perpendicular to the direction of the field.

The curl of vector F at a point P can be visualized by inserting a small paddle wheel into the field (interpreting the vector F as a force field) and see if the paddle wheel rotates or not. If there is an imbalance of the force on the sides of the paddle wheel, the wheel will rotate and the curl of F is in the direction of the wheel axis (according to the right hand rule). If the forces on both sides are equal, there is no rotation, and the curl is zero. The magnitude of the rotation velocity represents the magnitude of the curl of F at P. The curl of the vector field F is therefore a measure of the circulation of F around point P.

$(\nabla \times F)_p \rightarrow$ out

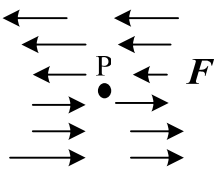

$(\nabla \times F)_p \rightarrow$ in

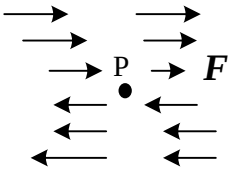

$$\left(\nabla \times F\right)_p = 0$$

According to Ampère's law in differential form,

$$\nabla \times H = J \qquad \text{Eq. 2-15}$$

the curl of the magnetic field is zero in a current-free region ($J=0$) and non-zero in a region where current is present. Thus, the curl of the magnetostatic field locates the source of the field (steady current).

According to Faraday's law in differential form,

$$\nabla \times E = 0 \qquad \text{Eq. 2-16}$$

the curl of the electrostatic field is always zero.

2.3.2 Static fields and potentials

Fields with zero curl are defined as lamellar or irrotational fields. All electrostatic fields are lamellar fields. According to the identity,

$$\nabla \times \nabla f = 0 \qquad \text{Eq. 2-17}$$

electrostatic field can be written as the gradient of some scalar (electric scalar potential V).

$$E = -\nabla V \qquad \text{Eq. 2-18}$$

In a similar fashion, in a current-free region ($J=0$), the magnetic field is lamellar ($\nabla \times H = 0$) so that the magnetic field may also be written as the gradient of some scalar.

$$H = -\nabla V_m \qquad \text{Eq. 2-19}$$

where V_m is the magnetic scalar potential.

Fields with zero divergence are defined as solenoidal or rotational fields. All magnetostatic fields are solenoidal based on Gauss's law for magnetic fields.

$$\nabla \cdot B = 0 \qquad \text{Eq. 2-20}$$

According to the vector identity

$$\nabla \cdot \left(\nabla \times F\right) = 0 \qquad \text{Eq. 2-21}$$

magnetostatic fields can be written as the curl of some vector (magnetic vector potential A).Thus, we may write

$$\nabla \cdot B = 0 \quad \Rightarrow \; B = \mu H = \nabla \times A \quad \Rightarrow \; H = \frac{1}{\mu} \nabla \times A \qquad \text{Eq. 2-22}$$

Inserting the magnetic field expression into the differential form of Ampère's law gives

$$\nabla \times H = J \quad \Rightarrow \; \nabla \times \left(\frac{1}{\mu} \nabla \times A \right) = J \quad \Rightarrow \; \nabla \times \nabla \times A = \mu J \qquad \text{Eq. 2-23}$$

The curl operator satisfies the following vector identity:

$$\nabla \times \nabla \times F = \nabla \left(\nabla \cdot F \right) - \nabla^2 F \qquad \text{Eq. 2-24}$$

where the last term in the previous equation is defined as the vector Laplacian. The equation defining the magnetic vector potential in terms of the current density becomes

$$\nabla\left(\nabla\cdot A\right) - \nabla 2A \;=\; \mu J \qquad \text{Eq. 2-25}$$

We are free to choose the characteristics of the vector potential to simplify the mathematics, so long as the fields defined in term of A still satisfy Maxwell's equations. If we choose

$$\nabla\cdot A = 0 \qquad \text{Eq. 2-26}$$

then the equation for the magnetic vector potential in term of the current density becomes

$$\nabla 2A \;=\; -\mu J \qquad \text{Eq. 2-27}$$

This equation is the vector analogy to Poisson's equation

$$\nabla 2V \;=\; -\frac{\rho_v}{\varepsilon} \qquad \text{Eq. 2-28}$$

In the case of 2D planar problems, we have the following equations:

$$J \;=\; \begin{bmatrix} 0 \\ 0 \\ j(x,y) \end{bmatrix} \qquad A \;=\; \begin{bmatrix} 0 \\ 0 \\ A_z{=}a(x,y) \end{bmatrix} \qquad B \;=\; \nabla\times A \;=\; \begin{bmatrix} \frac{\partial A_z}{\partial y} \\ -\frac{\partial A_z}{\partial x} \\ 0 \end{bmatrix}$$

The Partial differential equation (PDE) that the axis component of the magnetic vector potential verifies, is:

$$\nabla\cdot\left(\frac{1}{\mu\left(\left|B\right|\right)}\nabla A_z\left(x,y\right)\right) + j\left(x,y\right) \;=\; 0 \qquad \text{Eq. 2-29}$$

We notice that the magnetic permeability depends on the magnitude of the flux density B in saturable area (iron) so we obtain a nonlinear PDE to solve.

The advantage of using the vector potential formulation is that all the conditions to be satisfied have been combined into a single equation. If A is found, B and H can then be deduced by differentiating A. In addition, the form of the last equation is elliptic partial differential equation, arises in the study of many different types of engineering phenomenon. There are a large number of tools that have been developed over the years to solve this particular problem.

2.3.3 Time-varying Problems (Harmonic problems)

In this paragraph, we deal only with time harmonic problems. Harmonic problems are characterized by a sinusoidal dependence of all the quantities versus time. Thus it is interesting to introduce the complex representation of the sinusoidal variables in the following way :

If: $g(t) = 2G\cos(\omega t)$, we can write: $g(t) = 2\,\mathrm{Re}\left[G\exp(j\omega t)\right]$

and so: $$\frac{\partial g(t)}{\partial t} \Rightarrow j\omega G \qquad \text{Eq. 2-30}$$

This representation is applied to all the electromagnetic quantities varying with time. For example, we have the following notations in 2D planar problems:

Electric field: $e(x, y, t) = 2\,\mathrm{Re}\left[E(x, y)\exp(j\omega t)\right]$

Magnetic field: $h(x, y, t) = 2\,\mathrm{Re}\left[H(x, y)\exp(j\omega t)\right]$

Magnetic flux density: $b(x, y, t) = 2\,\mathrm{Re}\left[B(x, y)\exp(j\omega t)\right]$

Electric current density: $j(x, y, t) = 2\,\mathrm{Re}\left[J(x, y)\exp(j\omega t)\right]$

We will omit the notation (x,y) in the following in order to simplify the text.

If the field is time-varying, eddy currents can be induced in materials with a non-zero conductivity. Several other Maxwell's equations related to the electric field distribution must also be accommodated. The electric field E and the current density J still obey the constitutive relationship:

$$j(t) = \sigma\ e(t) \Rightarrow J = \sigma E \qquad \text{Eq. 2-31}$$

The induced electric field then obeys:

$$\nabla\times e(t) = -\frac{\partial b(t)}{\partial t} \Rightarrow \nabla\times\mathrm{E} = -j\omega\mathrm{B} \qquad \text{Eq. 2-32}$$

Substituting the vector potential form of B yields:

$$\nabla\times e(t) = -\frac{\partial}{\partial t}\left[\nabla\times a(t)\right] \Rightarrow \nabla\times\mathrm{E} = -j\omega\nabla\times\mathrm{A} \qquad \text{Eq. 2-33}$$

In the case of 2-D problems, the integration of this equation gives:

$$e(t) = -\frac{\partial a(t)}{\partial t} - \nabla v(t) \Rightarrow \mathrm{E} = -j\omega\mathrm{A} - \nabla V \qquad \text{Eq. 2-34}$$

which yields:

$$j(t) = -\sigma\frac{\partial a(t)}{\partial t} - \sigma\nabla v(t) \Rightarrow J = -j\omega\sigma\mathrm{A} - \sigma\nabla V \qquad \text{Eq. 2-35}$$

where V is an electric potential that may be given by an external source.
Finally, we obtain the following partial differential equation:

$$\nabla\times\left(\frac{1}{\mu(b(t))}\nabla\times a(t)\right) = j_{src} - \sigma\frac{\partial a(t)}{\partial t} - \sigma\nabla v(t) \qquad \text{Eq. 2-36}$$

$$\Rightarrow \nabla\times\left(\frac{1}{\mu(\mathrm{B})}\nabla\times\mathrm{A}\right) = J_{src} - j\sigma\omega\mathrm{A} - \sigma\nabla V \qquad \text{Eq. 2-37}$$

$$\nabla\times\left(\frac{1}{\mu(\mathrm{B})}\nabla\times\mathrm{A}\right) = -\sigma\mathrm{A} - \sigma\nabla V + J_{src} \qquad \text{Eq. 2-38}$$

where J_{src} represents the applied currents sources. The ∇V term is an additional voltage gradient that, in 2-D problems, is constant over a conducting body.

2.3.4 Boundary Conditions

Some discussion of boundary conditions is necessary so that we will be sure to define an adequate number of boundary conditions to guarantee a unique solution of the PDE. Boundary conditions come in three flavors :

2.3.4.1 Dirichlet. In this type of boundary condition, the value of A is explicitly defined on the boundary, e.g. $A = 0$. The most common use of Dirichlet-type boundary conditions is to define $A = 0$ along a boundary to keep flux from crossing the boundary.

2.3.4.2 Neumann. This boundary condition specifies the normal derivative of A along the boundary. Usually, $\partial A/\partial n = 0$ is defined along a boundary to force flux to pass the boundary at exactly a 90º angle to the boundary. This sort of boundary condition is consistent with an interface with a very highly permeable metal.

2.3.4.3 Mixed. The mixed boundary condition is a mix between Dirichlet and Neumann, prescribing a relationship between the value of A and its normal derivative at the boundary. An example of this boundary condition is : $\frac{\partial \mathrm{A}}{\partial n} + c\mathrm{A} = 0$. This boundary condition is most often used in eddy current problems on interfaces with bodies with small skin-depth eddy currents.

If no boundary conditions are explicitly defined, each boundary defaults to a $\partial A/\partial n = 0$ Neumann boundary condition. However, a non-derivative boundary condition must be defined somewhere so that the problem has a unique solution.
For axisymmetric problems, $A = 0$ is enforced on the line $r = 0$. In this case, a valid solution can be obtained without explicitly defining any boundary conditions, as long as part of the boundary of the problem lies along $r = 0$.

There are other types of boundary conditions that we can introduce in a numerical process in order to reduce the size of the problems: periodic and anti periodic conditions.

2.4 Numerical methods for elliptic PDE's resolution

2.4.1 Introduction

The analytic solution of electromagnetic PDEs presents some difficulties if the geometry is complex and the problem is nonlinear. Some numerical methods are developed to solve some kinds of PDEs. Some of them are listed in the following:

2.4.1.1 Finite difference method: This method uses the discretization of the partial derivatives onto the second order. The PDE is then solved as a linear equation. The main advantage of this method is its simplicity.

2.4.1.2 Finite elements method: The principle of this method consists on a discretization of the domain on polygonal domains (triangles for example) minimization of a function depending on the values of the unknown function on the nodes. This method presents the advantage that we can simulate every kind of geometries.

2.4.1.3 Boundary integral method: This method is based on the use of Green Formula. The solution of a harmonic function on a domain can be determined using the values of the function on the boundary of the domain. This method can be used for

magnetostatic problems with isotropic properties. It is so limited for some applications especially linear problems.

2.4.1.4 Hybrid Methods: These methods combine the finite elements methods in nonlinear eddy current area with boundary integral method in magnetostatic regions. The two problems are connected on the boundary between the two domains.

2.4.2 Basics of Finite Elements Method (FEM)

The two most popular methods of deriving the finite elements equations are the variational approach and the Galerking approach, which is a special case of the method of weighted residuals (MWR). The variational method was the first applied to problems in magnetics and occupies a large part of the early literature. Due to the greater generality of the weighted residual method, this method has increased its popularity. It is briefly presented here.

The MWR can be presented as follows. We begin with an operator equation

$$L(X) = 0 \qquad \text{Eq. 2-39}$$

on region Ω with boundary conditions on the boundary $\partial\Omega$. We substitute an approximate solution $\hat{X}$ into the previous equation. Since $X \neq \hat{X}$, we obtain a residual.

$$L(\hat{X}) = R \qquad \text{Eq. 2-40}$$

The MWR now requires that the integral of the projection of the residual on a special weighting function is zero over the domain of interest. The choice of the weighting function determines the type of MWR. In our case we will choose weighting function to have the same form as the finite element shape function. This is known as the Galerking method and will yields the same finite elements equation as the variational method in the case where the variational principle is known. As an example we take the time harmonic form of the diffusion equation with the z component of the magnetic vector potential A, as the unknown. For a linear 2D Cartesian problem:

$$\frac{1}{\mu}\frac{\partial^2 A}{\partial x^2} + \frac{1}{\mu}\frac{\partial^2 A}{\partial y^2} = -J_{src} + j\omega\sigma A \qquad \text{Eq. 2-41}$$

where μ is the magnetic permeability, ω is the angular frequency, σ is the electrical conductivity and J_{src} is the applied current density.

Substituting an approximation, $\hat{A}$, for A gives a residual

$$R = \frac{1}{\mu}\frac{\partial^2 A}{\partial x^2} + \frac{1}{\mu}\frac{\partial^2 \hat{A}}{\partial y^2} + J_{src} - j\omega\sigma\hat{A} \qquad \text{Eq. 2-42}$$

Multiplying by a weighting function and setting the integral to zero

$$\int_{\Omega} RW\,dxdy = 0 \qquad \text{Eq. 2-43}$$

Substituting for R

$$-\iint_{\Omega} W\left(\frac{1}{\mu}\frac{\partial^2 \hat{A}}{\partial x^2} + \frac{1}{\mu}\frac{\partial^2 \hat{A}}{\partial y^2}\right)dxdy + j\omega\sigma\iint_{\Omega} W\hat{A}dxdy = \iint_{\Omega} WJ_{src}dxdy \qquad \text{Eq. 2-44}$$

Integrating the first term by parts,

$$\iint_{\Omega} W\left(\frac{1}{\mu}\frac{\partial^2 \hat{A}}{\partial x^2} + \frac{1}{\mu}\frac{\partial^2 \hat{A}}{\partial y^2}\right)dxdy = \iint_{\Omega}\frac{1}{\mu}\left(\frac{\partial W}{\partial x}\frac{\partial \hat{A}}{\partial x} + \frac{\partial W}{\partial y}\frac{\partial \hat{A}}{\partial y}\right)dxdy - \oint_{\partial\Omega}\frac{1}{\mu}W\frac{\partial \hat{A}}{\partial n}dc$$

Eq. 2-45

where the last term is on the boundary $\partial\Omega$ with *n* being the outward normal unit vector. Substituting this result in Equation 2-44, we now break the surface integral into summation over small areas (triangular meshing). In this case, we will mesh the surface with triangles (the finite elements) and replace the integral over the entire domain with the summation of the integral over the individual triangles.

$$\sum_{M}\frac{1}{\mu^e}\iint_{\Omega e}\left(\frac{\partial W^e}{\partial x}\frac{\partial A^e}{\partial x} + \frac{\partial W^e}{\partial y}\frac{\partial A^e}{\partial y}\right)dxdy + j\sigma\omega\iint_{\Omega e} W^e\ A^e\ dxdy - \frac{1}{\mu^e}\frac{\partial A^e}{\partial n}\oint_{\partial\Omega e} W^e dc = J^e_{src}\iint_{\Omega e} W^e dxdy \qquad \text{Eq. 2-46}$$

where *M* is the number of triangular elements.

The line integral in the previous equation only needs to be evaluated over elements which have a side in common with the boundary of the problem. Normally this integral is simply set to zero implying that $\frac{\partial A}{\partial n} = 0$ witch results in the so called natural boundary condition. However, this integral is often used in problems in which the finite elements method is coupled to other solution techniques. In this case the integral must be evaluated.

Consider a triangular element depicted in the Figure 2-3

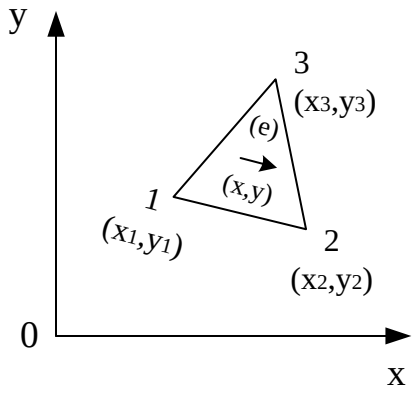

FIGURE 2-3 Triangular element

We will adopt the convention of clockwise numbering of the vertices. The vertices are nodes at which the unknown vector potential will be calculated.

If we assume that the potential varies linearly in the element, we obtain what is known as a linear or first order element. With this approximation, we may express the vector potential at any point in the triangle as:

$$A(e) = C_1 + C_2 x + C_3 y \qquad \text{Eq. 2-47}$$

where $C_1 + C_2 + C_3$ are constants to be determined. Note that since the vector potential varies linearly, the flux density, which is the derivative of the potential vector, is constant in the triangle.

At node i (1, 2 or 3), we have $x = x_i$ and $y = y_i$. At this point $\hat{A}$ must be equal to $\hat{A}_i$, so that

$$\hat{A}_i = C_1 + C_2 x_i + C_3 y_i \qquad i = 1..3 \qquad \text{Eq. 2-48}$$

This gives three equations and three unknowns that can be easily determined.

We can express the magnetic vector potential as:

$$A(e) = \frac{1}{2\Delta}\sum_{i=1}^{3}(a_i + b_i x + c_i y)\,\hat{A}_i \equiv \sum_{i=1}^{3} N_i(x,y)\hat{A}_i \qquad \text{Eq. 2-49}$$

where the coefficients of the nodal potentials are called shape function.

$$N_i = \frac{a_i + b_i x + c_i y}{2\Delta} \qquad \text{Eq. 2-50}$$

with:

$$a_i = x_k y_m - x_m y_k$$
$$b_i = y_k - y_m$$
$$c_i = x_m - x_k$$
$$\Delta = (a_i + a_k + a_m)/2 \text{ : surface of the triangle}$$

The subscripts (i, k, m) represent all circular permutations of the subscripts 1, 2, 3 in the clockwise numbering.

These functions have the following important properties:

$N_i = 1$ at the node i and is 0 at all others.

The sum of all the shape functions at any point in the triangle is 1.

The substitution of these shape functions in Equation 2-46 leads to a linear system of the form:

$$MA = F$$

where M is a stiffness matrix,
A is a nodal magnetic potential vector,
F is a source vector.

The general term of M_{ik} is computed by integrating the functions over all the elements connected to the nodes i,k:

$$Mik = \sum_{\substack{\text{connected}\\ \text{elements}}} \iint_{(e_i)n} \frac{1}{\mu_r}\frac{b_i b_k + c_i c_k}{4\Delta^2}\,dxdy$$

$$= \sum_{\substack{connected \\ elements}} \frac{1}{\mu_r} \frac{b_i b_k + c_i c_k}{4\Delta} \qquad \text{Eq. 2-51}$$

(This formula is for magnetostatic problem $\omega = 0$)

Considering that the current density is constant on each element, the general term F_i of the vector F is:

$$F_i = \sum_{\substack{connected \\ elements}} \mu_0 J_i \iint_{(e_i)n} N_i \, dxdy = \frac{\mu_0}{3} \sum_{\substack{connected \\ elements}} J_i \Delta_i \qquad \text{Eq. 2-52}$$

This linear system presents the following characteristics:

a. it is symmetrical,

b. the matrix M comprises a strong percentage of null terms, because is calculated only if node i is connected to the node k; thus it is beneficial to concentrate these terms around the principal diagonal of M, which confers a structure-band made profitable to reduce the cost of resolution of the system.

2.4.3 Assembly

Once the element matrices are found for each element they are used to form the global or system matrix in a process known as assembly. The process is quite simple and is illustrated in the example which follows. Each element matrix has rows and columns corresponding to the nodes into the element. In the assembly process we simply add all of the element matrices together to form the global matrix. For a problem with m nodes we begin with an m*m zero matrix. We then go though each element and add the ij term in the global matrix. The resulting global matrix will be spare symmetric and singular.

2.4.4 General structure of a FEM software

A finite elements software for electromagnetic (electrical machinery) is generally made up of three parts called commonly: “pre-processor”, “processor”, and “post-processor”. With this three blocks, it is possible to add the “mesh generator”, generally it is integrated into the processor, but it carries out a specific and can be extracted from it.

2.4.4.1 The pre-processor

The pre-processor is used to draw the geometry of problems, to define materials and to define state of border. The drawing of a geometry validates is usually composed of four tasks not necessarily sequential:

a) Draw: allows to draw the geometry of the problem by defining the end points of the lines and segments of arc which make a diagram then by connecting them by segments or arcs.

b) Materials: allows to define the physical characteristics of the various geometrical areas previously drawn in their assigning properties (magnetic linear or not, conductivity…). This action also allows to define the precision of the grid. One can also introduced the densities of current sources if a section of a conductor is represented.

c) Circuits: in the same way that for materials, it is possible to define circuits linked to voltage or power sources. It is possible to specify the number of turns and the value of the amplitude of the current or the voltage applied.

d) Boundary conditions: these conditions can be of type Dirichlet, Neumann, periodicals, antiperiodic. They are applied to the external edges of the geometry.

2.4.4.2 The processor

The “processor” is the element which solves the partial differential equation in its discrete form. In practice, one solves a linear system by a given method of resolution (Factorization LU, Cholesky, method of the combined gradient…) For the nonlinear problems, the processor solves in an iterative way until the required precision is reached. Thus, the processor makes it possible to know the value of the magnetic potential vector in each node of the grid and thus a linear approximation inside each elements of the same grid. Once this variable is determined, it is easy to deduce the other quantities (magnetic field, flux density,…).

2.4.4.3 The post-processor

The “post-processor” is the element which analyzes the results and exploits it. A visualization aspect is often useful for the comprehension of the results. It is possible that the post-processors visualizes the line of induction, the threads of current or the levels of induction or the density of current. These visualizations can be made one the whole structure or on a part of it. It is also possible to calculate quantities on a domain or along a line. It is then possible to calculate a force or a torque by the use of the calculation of the constraints Maxwell tensor along a line. Another interesting quantity can be the average of induction etc… For a domain one can calculate resistive losses or energy, etc…

A software FEMM (Finite Elements Method in Magnetic) is used in this thesis.

2.5 Chapter summary

The chapter describes the fundamental of electromagnetism required for the modelling of electromagnetic devices. Boundary conditions are discussed. Galerking approach for numerical solution is introduced in conjunction with the software FEMM.

CHAPTER 3
DESIGN AND CONSTRUCTION OF THE PM MACHINE

3.1 The parameters of PMSM

For the design of the Permanent Magnet Synchronous Motor (PMSM), we construct the permanent magnet rotor based on the stator frame of a three-phase induction motor without changing the geometry of stator and the winding. The specification and geometry are shown in Table 3-1.

TABLE 3-1 Specification and Geometry of the motor

Designation	Unit	value
Speed	rpm	1500
Frequency	Hz	50
Number of pole	-	4
Stack length	mm.	51.4
Internal diameter	mm.	90
External diameter	mm.	146
Air-gap (*e*)	mm.	1
Number of slot	-	36
Number of slot/pole/phase (q)	-	3/pole/ph

3.2 Magnetic materials

The development of the permanent magnet materials began in the early 20th century, first with magnetic steel [4]. In the 1930's the first material was developed which was useful for electro-mechanical devices. This was an aluminum-nickel-cobalt alloy AlNiCo which is still used in special applications but with decreasing importance. Its major drawback is a low coercive force Hc. The next step was the development of ferrite permanent magnets (mostly SrO $6(Fe_2O_3)$) in the 1950's which were significantly cheaper and had remarkably higher coercive force and energy product $(BH)_{max}$ than earlier materials. Until today this is the leading magnet material due to its superior price-performance ratio. Well known applications are for instance loudspeakers and small DC motors. Also larger machines with ferrite magnets were constructed but due to the relatively low remanence Br, it has been difficult to reach a sufficiently high air-gap flux density for high performance machines.

The next milestone in advances of permanent magnetism was the development of sintered rare-earth cobalt magnets around 1970, in particular samarium-cobalt alloys SmCo. These offered high remanence and high coercive force resulting in a significantly higher energy product than ferrites can achieve. These properties and the large reversible demagnetization range (high intrinsic coercive force Hci) made these magnets to be the superior choice for high performance machines. However, the high price of the raw materials has prohibited a large scale use. Hence major efforts were undertaken to find a magnet material with as good properties but constituted of cheaper raw materials. This research led to the, nowadays well known, neodymium-iron-boron NdFeB magnets, introduced in 1983. Although cheaper than SmCo and of even higher energy density, NdFeB is not always superior due to its lower thermal stability, caused by the lower Curie temperature, and its reactivity which leads for

instance to corrosion problems. In contrary to ferrites the conductivity of rare-earth alloys can yield eddy current losses. Some of these problems can be overcome by embedding the rare-earth powders in a matrix, for instance resin or, for flexible magnets, rubber (also used with ferrite powder). Figure 3-1 shows a qualitative hysteresis curve of a magnet grade suitable for PM machines. Besides an illustration of the mentioned magnetic properties this figure also introduces the limits for irreversible demagnetization, HD, BD. Figure 3-2 illustrates the advances of permanent magnet materials. Today high performance rare-earth magnets are most widespread in small motors, especially hard disk drives. The application in high power devices has so far become common in servo drives while larger PM machines are just on the threshold of their commercial introduction.

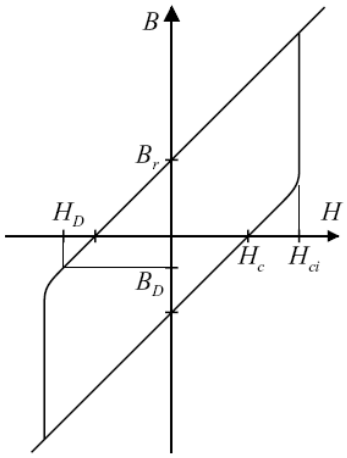

FIGURE 3-1 Principal hysteresis curve of permanent magnet material

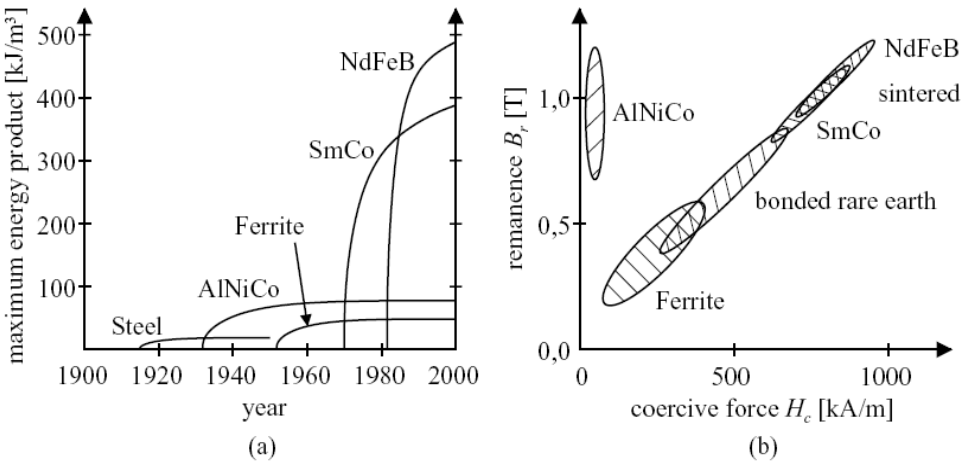

FIGURE 3-2 The advances of permanent magnet materials

(a) Development of magnet materials energy product

(b) comparison in terms of remanence and coercivity at room temperature

Figure 3-3 and Figure 3-4 show the B-H curve of the magnet and iron.

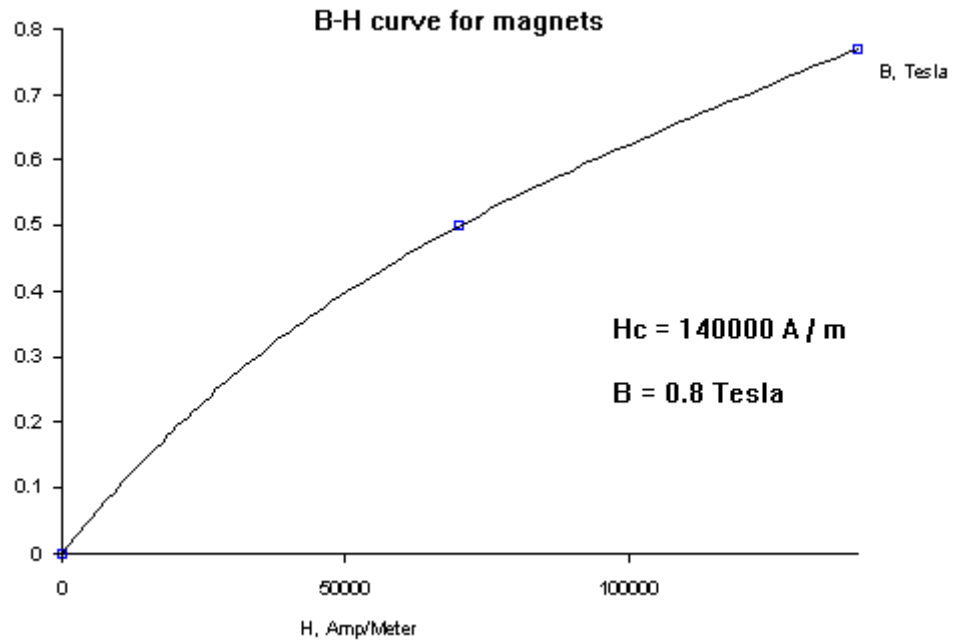

FIGURE 3-3 B-H curve of magnet (NdFeB)

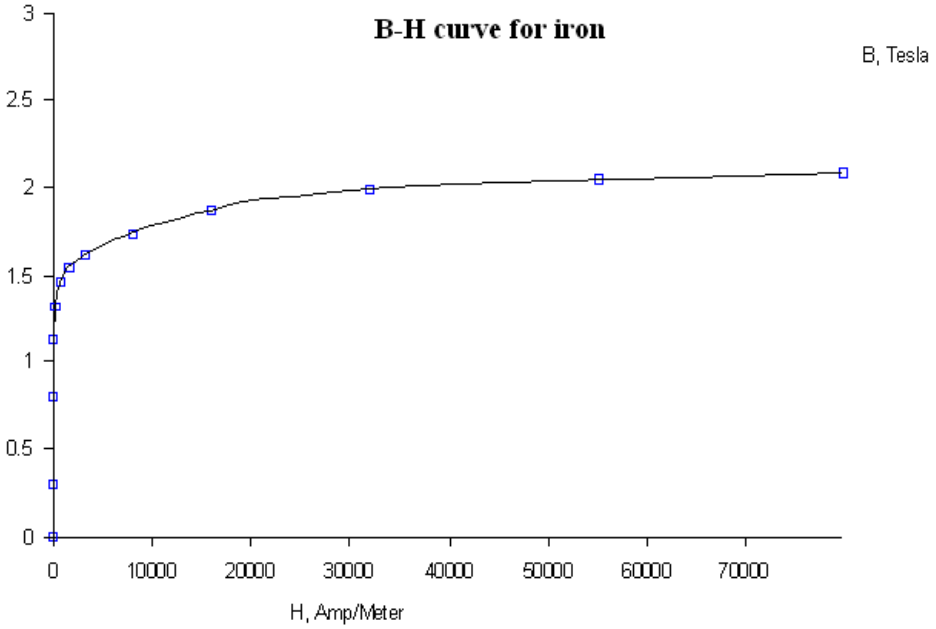

FIGURE 3-4 B-H curve of iron (M-19 steel)

Besides the further increase of maximum energy product and remanence, the topic of recent research is also to increase the Curie temperature of NdFeB alloys. This results in improved properties at elevated temperature which is particularly important in high performance motor applications. The common approach is to partly substitute neodymium by dysprosium, iron by cobalt and molybdenum, and boron by aluminum. The addition of different elements shows various influence on remanence and intrinsic coercive force, their temperature coefficients, and the Curie temperature. However, the price usually rises. An alloy with high remanence at room temperature has usually a comparably low intrinsic coercive force and high temperature coefficients of the magnetic properties. This leads to a higher demagnetization risk and thus magnet grades with lower maximum energy product but relatively high temperature stability must be chosen for high performance electrical machines. In this context it should be noted that the temperature coefficient of SmCo alloys is remarkably lower than that of NdFeB. Therefore a SmCo magnet remanance flux density, which is weaker at room temperature, can be stronger than a comparable NdFeB magnet at elevated temperature.

What all these magnets have in common is the low permeability, similar to air. The relative permeability for NdFeB magnets is typically about $\mu_r = 1.05$ (see also Figure 3-5). A problem of NdFeB magnets is their reactivity. This leads to corrosion and subsequently loss of magnetic properties. Therefore these magnets are often coated, for instance with nickel, increasing the costs for the magnets. An alternative is to ensure complete sealing in the motor production process. This can for example be achieved by embedding the magnets entirely in resin. In this case it is however important to avoid too much exposure to air and moisture for a period of time starting from the production of the magnets to their assembly which complicates the handling remarkably. McCaig and Clegg gave an example for the corrosion of NdFeB magnets. Although not all conditions of the test are revealed it may give an indication of the severity of this problem: “When NdFeB magnets are kept at a temperature of 60°C in a relative humidity of 90% for 300hr there is a flux loss due to corrosion of more than 2%.”

In most properties SmCo magnets are superior to NdFeB magnets. Only the maximum energy product at room temperature is higher for NdFeB. However, the high price of SmCo normally prohibits its use in larger commercial drives. For special applications the increased price can be justified, for instance in high performance servo drives. Figure 3-5 shows the demagnetization curves of a high temperature, uniaxially pressed NdFeB magnet.

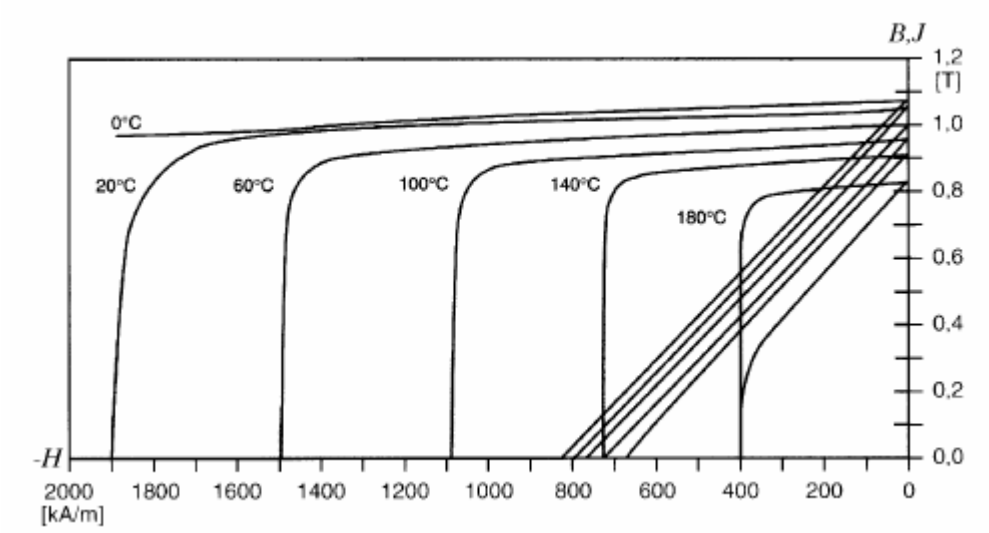

FIGURE 3-5 Demagnetization curves of an uniaxially pressed high temperature NdFeB magnet

Not only the metallurgical composition determines the properties of sintered magnets. In contrary some attention should also be paid to the production process. The different processes on the production of anisotropic sintered magnets are illustrated in Figure 3-6. After the fabrication of the alloy powder it is pressed and the grains are oriented by a magnetic field. This grain orientation should not be confused with the magnetization process. However, this orientation determines the direction of the magnetic polarization that will follow the magnetization process. Radially magnetized arc-shaped magnets can be realized as depicted in Figure 3-6. The pressing is either done uniaxially, typically using a hydraulic press, or isostatically where the pressure is applied from all directions, for instance in a hydrostatic pressure container. Today the uniaxial pressing is the most common method since it is preferable for automated manufacturing and allows more complex magnet shapes. In this process the maximum size of a magnet is determined by the force the hydraulic press can deliver because a certain force per area is required. Since the magnets are brittle also the side length ratios must stay within reasonable limits. Alternative to uniaxial, isostatic pressing is used, especially for larger magnet blocks. An advantage is that a higher maximum energy product can be achieved for the same alloy. After orientation and pressing the magnets are sintered and undergo a heat treatment. Afterwards machining, typically grinding, is usually required to obtain the exact magnet shape and dimensions. It should be noted that this machining is far more complex for arc-shaped magnets than for simple bars and also the material loss is much higher. Consequently the price per weight is much higher for magnets of more complex shapes and it is therefore recommendable to use a larger number of small bar-shaped magnets instead. Besides grinding, also slicing of large, isostatically pressed magnet bars is utilized. The last step in the magnet production is the magnetization. For this purpose a quite high flux density of approximately 3.5T is required, yet a rather short pulse is sufficient. Magnets with radial orientation can also be magnetized in a linear field if the component along the predefined orientation is sufficiently high. Not always is the magnetizing performed immediately after the

production. Often it is preferable to delay the magnetizing until the magnets are assembled. This simplifies transportation and handling but makes the magnetization process more difficult.

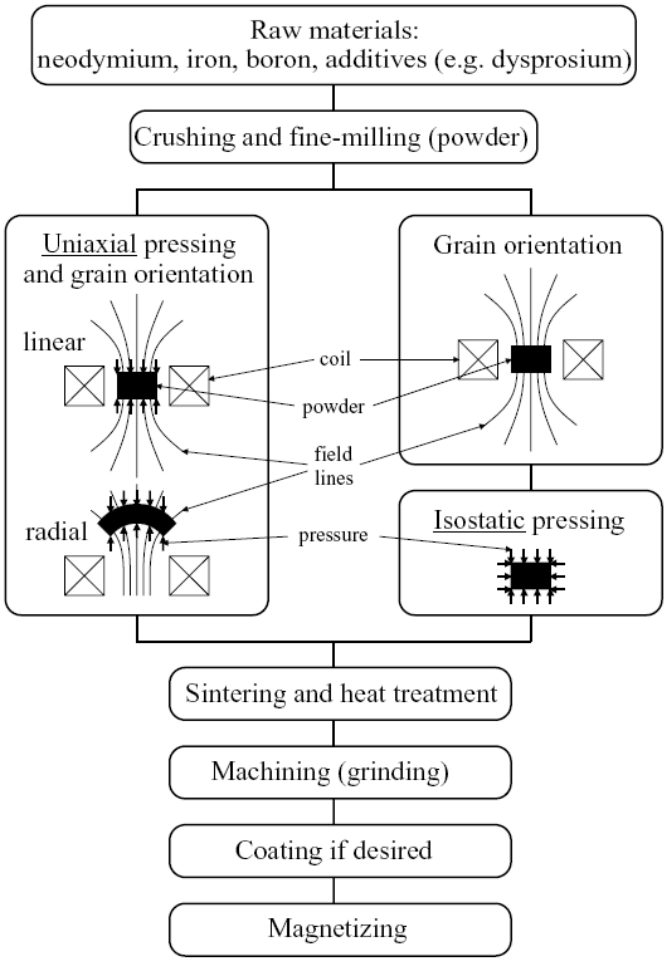

FIGURE 3-6 Production process of sintered, anisotropic NdFeB magnets

Great care is required when handling magnetized material. Besides the high forces there is also the risk that the brittle magnets can burst. Consequently gloves and goggles should be compulsory. Furthermore, when machining NdFeB magnets caution must be taken due to the high reactivity and inflammability of the powder. Even irritations of the respiratory organs can occur.

Samarium Cobolt Magnets (SmCo) are used in this thesis which are also part of the rare earth family. The compound of Samarium Cobalt was discovered in 1966 by Dr. Karl J. Strnat [5]. They were once the most powerful permanent magnet, but NdFeB magnets have surpassed them. Samarium cobalt is a powdered metal which is compacted when it is near a magnetic field and then sintered. Sintered means that when a compacted powder magnet is exposed to heat treat operation, the full density and magnetic orientation can be attained. SmCo magnets have also a very strong

magnetic field. They tend to resist demagnetization extremely well. Unlike Neodymium magnets, it is also very corrosion resistant. SmCo magnets can operate at higher temperatures up to 300°C and are widely used in applications in which higher operating temperature and higher corrosion and oxidation resistance are crucial. The temperature coefficient of remanence is usually less than ±0.05%.Two common compositions of SmCo magnets are $SmCo_5$ and Sm_2Co_{17}. They can be sintered and bonded. Generally, the cost of SmCo magnets is higher than NdFeB magnets. But NdFeB magnets are stronger than SmCo magnets.

FIGURE 3-7 SmCo magnets (Samarium Cobalt)

Material Information

1. An alloy compose of SmCo5/Sm2Co17 produce by powder metallurgical method
2. Extremely hard & brittle
3. High demagnetization resistance
4. Excellent anti-corrosion properties
5. More expensive than NdFeB magnets because of limited raw material supply
6. Outstanding thermal stability

Typical Physical Properties

Curie Temperature (°C)	700-800
Maximum Operating Temperature (°C)	350
Resistivity (μ ohm.cm)	50-90
Hardness (Hv)	450-600
Density (g/cm3)	8.0-8.5
Relative Recoil Permeability (μrec)	1.10
Saturation Field Strength, kOe (kA/m)	37.5 (3000)
Temperature Coefficient of Br (%/°C)	-0.05 ~ -0.03
Temperature Coefficient of iHc (%/°C)	-0.25 ~ -0.19

TABLE 3-2 Magnetic Properties of SmCo Magnets (Samarium Cobalt)

Material	Grade	Remanence		Coercivity		Intrinsic Coercivity		Max. Energy Product	
		Br(mT)	Br(kGs)	bHc(kA/m)	bHc(kOe)	iHc (kA/m)	iHc (kOe)	(BH)max (KJ/m^3)	(BH)max (MGOe)
$SmCo_5$	S 16	750-800	7.5-8.0	557-637	7.0-8.0	1989	25	111-143	14-18
	S 18	800-930	8.0-9.3	597-677	7.5-8.5	1432	18	127-159	16-20
	S 20	850-980	8.5-9.8	597-677	7.5-8.5	1273	16	143-175	18-22
	S 24	1000	10.0	680	8.5	1195	15	175-190	22-24
Sm_2Co_{17}	S 180	900-1030	9.0-10.3	597-677	7.5-8.5	1194	15	127-159	16-20
	S 22A	900-1030	9.0-10.3	613-693	7.7-8.7	1989	25	159-191	20-24
	S 22B	900-1030	9.0-10.3	613-693	7.7-8.7	1432	18	159-191	20-24
	S 240	980-1080	9.8-10.8	636-716	8.0-9.0	1432	18	175-207	22-26
	S 26A	1000-1130	10.0-11.3	676-756	8.5-9.5	1194	15	191-223	24-28
	S 26B	1000-1130	10.0-11.3	676-756	8.5-9.5	796	10	191-223	24-28
	S 280	1030-1130	10.3-11.3	716-796	9.0-10.0	1432	18	207-239	26-30
	S 270	1000-1100	10.0-11.0	357-516	4.5-6.5	413	5.2	183-223	24-28
	S 300	1100-1200	11.0-12.0	438-517	5.5-6.5	454	5.7	223-255	28-32

Typical Demagnetization Curves of SmCo Magnets (Samarium Cobalt Magnets)

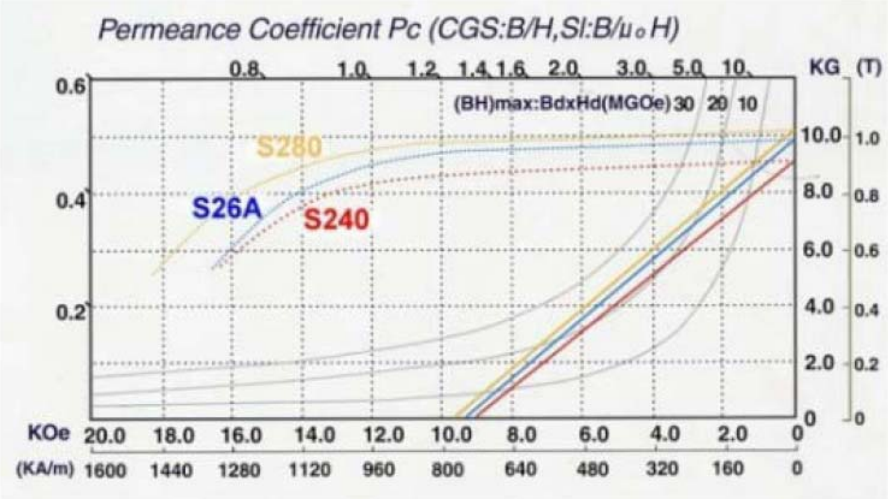

FIGURE 3-8 Demagnetization curves of SmCo magnet

An often used, although not optimal, approach to the design of PM machine is to start from a classical asynchronous or synchronous motor design and replace the rotor by a permanently magnetized variant [4]. This leads immediately to a cylindrical iron core with surface mounted magnets as shown in Figure 3-9(a). Alternatively the pole gaps can also be filled with iron yielding a surface inset magnet design shown on Figure 3-9(b). Bearing in mind that the permeability of the magnet is close to that of air it becomes evident that both versions have the same reluctance along the flux path of the direct axis. In contrary the reluctance along the quadrature axis is lower for the surface inset type. Consequently the surface mounted rotor is practically non-salient ($L_d = L_q$) while a saliency is obtained from the surface inset type. This saliency is inverse to that of wound field synchronous machines ($L_d<L_q$). On the pole edges of a

surface inset PM rotor a leakage of magnet flux will occur. Therefore the air-gap flux is slightly lower than that of a surface mounted rotor with the same magnets and the same air-gap length. If the saliency of the basic design is not as desired, internal flux barriers can be used to decrease the reluctance in any direction. In our case we choose the surface mounted PMs so $L_d = L_q$.

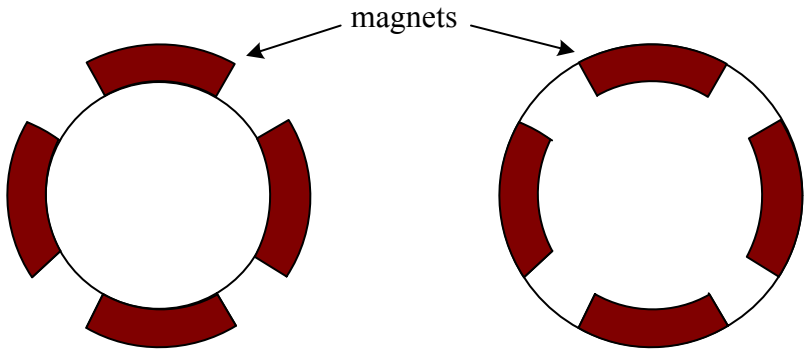

a) surface mounted magnets b) surface inset magnets

FIGURE 3-9 Basic cross sections of surface magnet rotors (4 poles)

The high remanence flux density of rare-earth magnet materials allows today the construction of high performance surface magnet motors. With ferrites it was not possible to achieve a sufficiently high air-gap flux density and thus the torque density of the machine was lower. Hence flux concentration designs with internal magnets were popular.

A beneficial alternative is banding with high tensile strength fibres. Typical materials are for instance glassfibre, carbon fibre, aramid and Kevlar[tm.], mostly plastic bonded. These fibres can offer higher tensile strength than steel. Furthermore no eddy currents are induced as they are not conductive. Their handling is however more complex. Besides the surface on which they are applied must be very smooth. This can easily be achieved for the surface inset design. For surface mounted magnets however, nonmagnetic fillers are required in the pole gaps. As the torque producing alignment forces act upon the magnets their transfer to the rotor core must also be considered. In that respect the surface inset design is clearly advantageous. Halfway inset magnets should also be considered. An inconvenience of plastic bonded materials is that their thermal conductivity is low restricting the cooling of the rotor surface. This should however not be necessary as the machine can be constructed to have very low rotor losses.

As rectangular magnets are significantly cheaper per volume than arc-shaped pieces it is recommendable to subdivide a pole into many rectangular pieces both in tangential and axial direction. Besides the cost reduction the eddy current losses in the magnets are also significantly reduced. Moreover, the axial subdivision enables the skewing of the rotor in steps which can be beneficial for suppressing torque ripple. Due to the increased amount of pieces of magnetized material the production expenses may increase. For large machine it is, however, impossible to produce magnet pieces large enough to form a pole unless the number of pole pairs is very high.

A significant advantage of surface magnet rotors is that almost no leakage of magnet flux occurs as no iron bridges exist which must be saturated. Consequently the required amount of magnet material is comparably low resulting in low costs. However, this benefit might be neutralized if arc-shaped magnets are needed. Furthermore the banding can be expensive, both in material and production aspects.

Since the main flux in the rotor is constant in a synchronous machine a solid steel rotor core is principally possible. However, time and space harmonics can cause eddy current losses. The time harmonic losses in a solid steel rotor can be kept low by a high inverter switching frequency like in the case of a steel retaining sleeve. On the other hand the slot space harmonics prohibit the use of solid steel for the rotor core of a surface inset design as the eddy current losses in the pole gap can become intolerably high. Moreover the rotor core can easily be made laminated with existing production facilities. Especially for larger machines a laminated rotor is recommendable as the stator core must be laminated anyway. Rotor and stator sheets can thus be punched together.

However this thesis has used the surface mount magnets instead of using surface inset magnets because it is easy to build the rotor.

3.3 Computation of the PMSM

3.3.1 Air-gap flux density.

For designing the stator geometry, methods can be utilized that are well established from e.g. asynchronous motor design [4]. This has therefore not been studied in the present work. The focus is rather on the permanent magnet rotor design and on special demands for utilizing the switched stator winding technique. Furthermore a slotted stator is assumed. The air-gap flux density is limited by the saturation of the stator core. In particular the peak flux density is limited by the width of the teeth while the stator back determines the maximum total flux. Besides the allowable saturation level is dependent on the application. Generally the flux density is lower in high efficiency machines and higher in machines designed for maximum torque density. The peak air-gap flux density lies typically in the range 0.7 – 1.1T. It should be noted that this is the total flux density, i.e. the sum of rotor and stator fluxes. This means that the rotor flux can be chosen higher if the armature reaction is smaller implying higher alignment torque. To achieve a great reluctance torque contribution however, the stator reaction must be large. The machine parameters give that a large ϕ_m and small inductances L, are required to obtain mainly alignment torque. This is usually desirable for operation below base speed as high inductances lower the power factor cos(φ).

When the maximum air-gap flux density is set the number of stator winding turns can be determined. For this purpose the fundamental air-gap flux density wave is considered. It has a predefined amplitude $\hat{B}_{g(1)}$ (0.7 – 1.1T).

The air-gap flux density from the magnets is defined which its fundamental amplitude $\hat{B}_{mg(1)}$ must be selected somewhat lower than $\hat{B}_{g(1)}$. As a guideline for the initial design step 70% of $\hat{B}_{g(1)}$ (0.5 – 0.8T) may be used if the machine is supposed to operate in field weakening since relative high inductances are required implying high stator reaction. If the machine shall however be optimized for operation below

base speed, 90% of $\hat{B}_{g(1)}$ (0.6 – 1.0T) might be a suitable start value as low inductances and low armature reaction are preferable which will be illustrated.

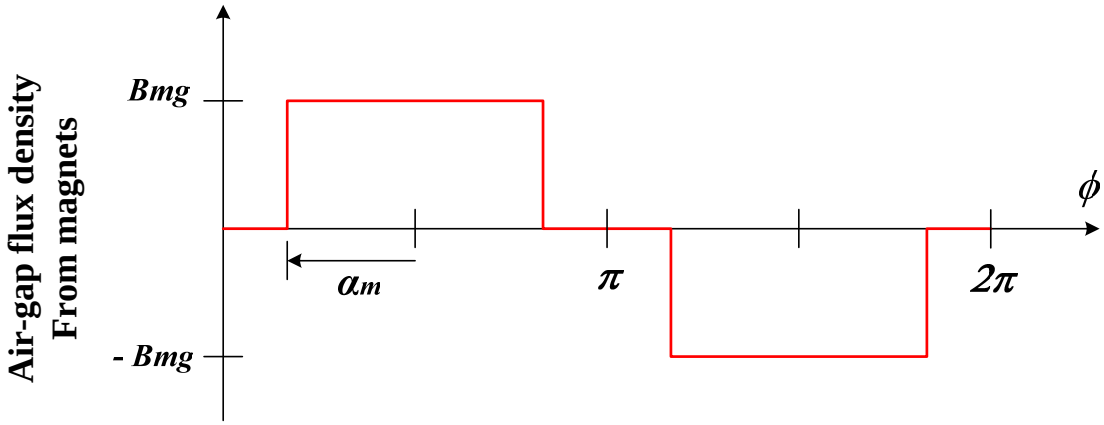

FIGURE 3-10 Magnet flux density distribution in the air-gap

3.3.2 Winding of the AC machines.

Winding described here are those of stators of synchronous and asynchronous machines, or of wound rotor of asynchronous machines [3]. They are intended to create, when one feeds them by a system of three-phase currents, a rotating magnetic field.

Case of a single wire

Consider a coil placed in two slots placed on opposite sides of the stator (diametrical winding), supplied by a current I. On the assumption that iron is infinitely permeable and that the effect of teeth is negligible, in normal flux density of air-gap will take the form described by the Figure 3-11.

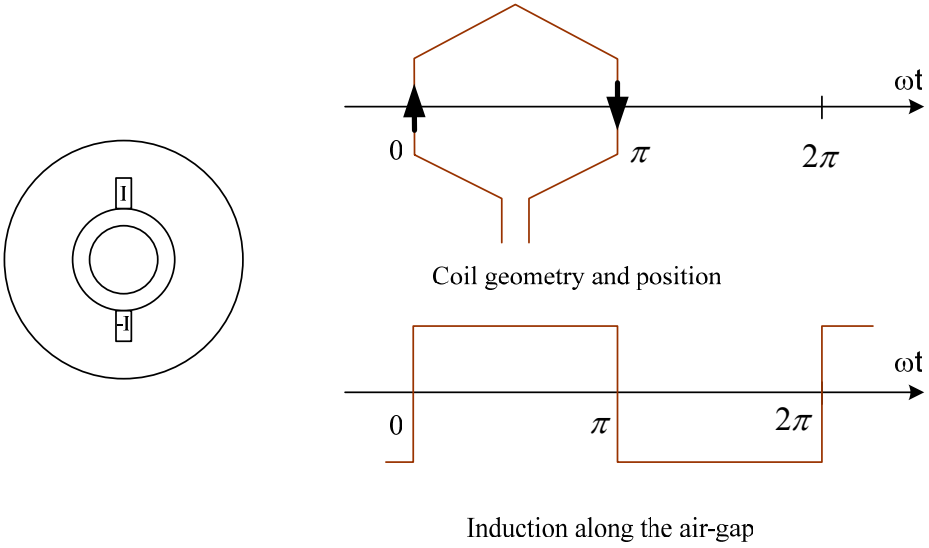

FIGURE 3-11 Winding geometry and position for a single coil

Distributed Winding

To obtain a curve B(θ) in the air-gap closer to its fundamental sinusoidal waveform than the preceding rectangular curve, one must replace the single coil by a distributed winding formed of several coils placed in series in consecutive slots. Let us suppose, indeed, that this distributed winding is made up for example of 3 wires, placed in 3 consecutive slots per pole pitch. To preserve the same total number of ampere turns per pole, each wire, in series with the others, is closed by a current of I/3 intensity. The winding geometry as well as the induction along the air-gap are represented in Figure 3-12.

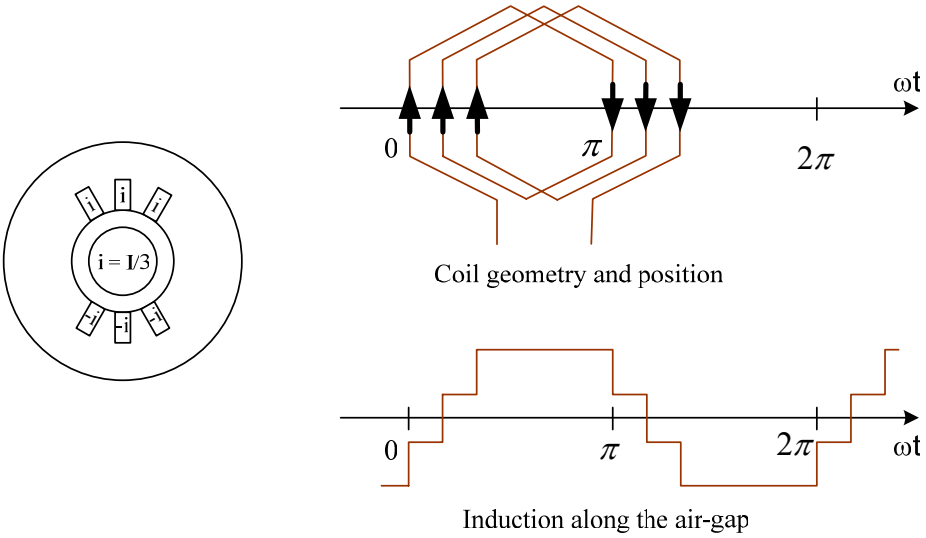

FIGURE 3-12 Winding geometry and position for a distributed winding

The waveform of the induction along the air-gap is in "staircase" and depends only on the distribution of the currents in the slots and not on the way of connecting the conductors ends. Thus, five diagrams of winding (6 slots per pole and phase) are, from the point of view of the creation of an electromagnetic field in the machine, strictly equivalent (Figure 3-13):

1. consequent-pole lap winding (Figure 3-13a)
2. consequent-pole concentric winding (Figure 3-13b)
3. separate concentric winding (Figure 3-13c)
4. separate lap winding (Figure 3-13d)
5. separate shortened lap winding (Figure3-13e)

These diagrams differ from the distribution the coils and from length of the coils ends.

These last only affect:

1. mass of copper used, and thus directly the cost;
2. ohmic voltage drops and linkage flux of the end windings;
3. cooling of these connections, which is often a significant criterion;
4. finally, simplicity of implementation in an industrial way as well as facility of insulation.

The choice of the diagram to be used in a machine for the distribution of the coils in the slots is then important. Some of the presented diagrams are only here for a didactic presentation and are never used. This is in particular the case of lab

diametrical schemes, with consequent (Figure 3-13a) or separate poles (Figure 3-13d), because they are difficult to implement, like for all overlapping windings, and also they are important copper consumer.

The other schemes are usually used. The concentric one with consequent-pole (Figure 3-13b), also an important copper consumer, must as far as possible be avoided, even if it is very easy to mechanize the insertion process as for a separate concentric winding(Figure 3-13c). The separate shortened lap winding(Figure 3-13e), is mainly used in the medium power range, because it makes possible to place identical coils with a perfect regular distribution of the coils heads. Moreover, it authorizes any step of winding, as well as irregular distributions (a fractional number of slots per pole and phase).

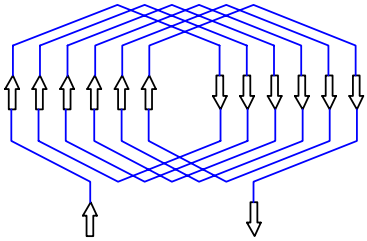

a) Consequent-pole lap winding

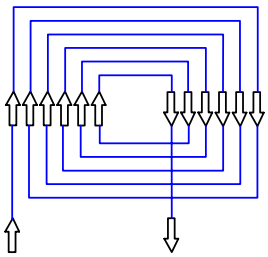

b) Consequent-pole concentric winding

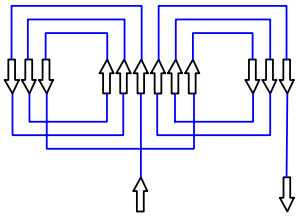

c) Separate concentric winding

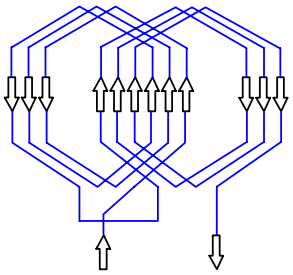

d) Separate lap winding

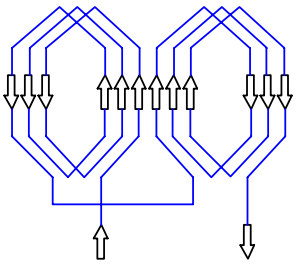

e) Separate shortened lap winding

FIGURE 3-13 Example of windings

End winding and stator resistance

Some possible machine structure sizes are illustrated in Figure 3-14. The machine with the air-gap diameter $D\delta$ equal to the length of the core L, is illustrated in a) with a conventional winding and b) with a concentrated fractional slot winding[6]. The end winding of the conventional lap winding a) is as long as the length of the core L. With fractional slot windings, shown in Figure 3-14b), the end winding length is about 1/5 of the length of the machine. In longer machines the relative end winding length may be much smaller than in short machines and, therefore, the end winding length may be a less important parameter in such cases. Figure 3-14c) shows a long machine, which has a higher pole number than the machine in Figure 3-14b).

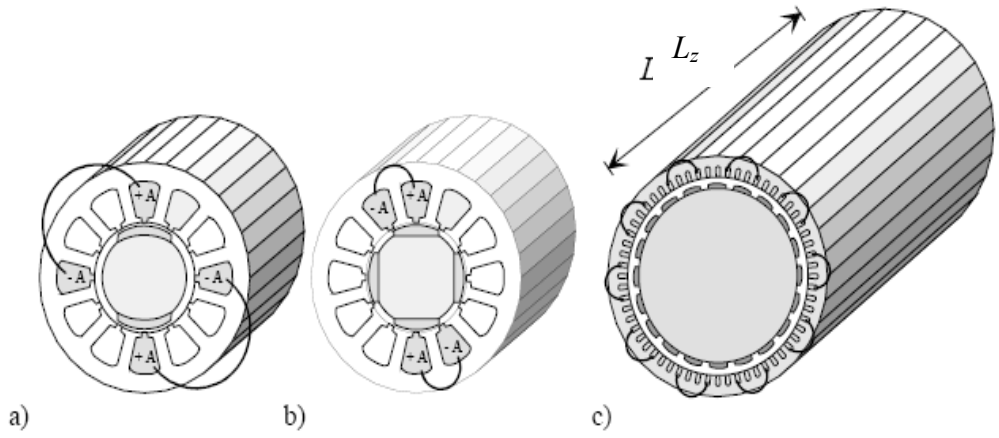

FIGURE 3-14 The machine structures.

a) conventional winding, where $p = 2$, $q = 1$
b) concentrated fractional slot winding, where $p = 4$, $q = 0.5$ (short machine)
c) a winding, where $q = 1$ and the pole number is high (long machine where the relative end winding length is short despite of the traditional winding).

3.3.3 The back-emf

The other one importance thing is back-emf waveform. A good estimate of the back-emf waveform is required for two main reasons. In the first place, it is an important indicator of the ability of the motor to produce smooth torque. Squarewave motors need a back-emf waveform that is essentially flat throughout the communication zone, while sinewave motors require essentially sinusoidal back-emf waveforms. In theory it is possible to profile the current waveform by chopping so that smooth torque is produced with any back-emf waveform, but this requires sophisticated electronics and is only occasionally proposed in practice. Most of the time, designers aim to get the back-emf waveform as close as possible to the trapezoidal or sinusoidal norms, within reasonable limits imposed by manufacturing constraints.

The second reason for requiring a good estimate of the back-emf waveform is for accurate simulation of the motor operating with its controller, and for the determination of the current waveform and the correct control strategy.

In this thesis we must know the back-emf of the machine, then we can compute the back-emf at no load as shown below.

From the value of specification given in Table 3-1, we have

L_z = 51.4 mm., f = 50 H_z, B_e = 0.857 T., p = 2, N_{turn} = 74 turns, 3 phase,

$\tau_p = \frac{2\pi Ra}{2p}$ = 70.68 mm. and then

$$\varphi_p \approx B_e \ \tau_p \ L_z \times \frac{2}{3} \qquad \text{Eq. 3-1}$$

$\approx$2.075 mWb. ; φ_p : flux per phase

$$\varphi = p \times \varphi_p \times N_{turns} \times phase \qquad \text{Eq. 3-2}$$

= 921 mWb.

$\varphi \approx 921 \text{ mWb} \times \cos(100\pi t)$

$E = \frac{\partial \varphi}{\partial t}$ = 289.57 V. ; V_p

= 204.726 V. ; V_{rms}

3.3.4 Computation the copper losses in the stator

From the equation of the copper losses

$$P_j = 3R_s I^2 \qquad \text{Eq. 3-3}$$

$$R_s = \rho \frac{L}{S} \qquad \text{Eq. 3-4}$$

where

L : Total length of the copper per phase

S : Cross section of the copper

ρ : resistivity of the copper has value 1.68×10^{-8} $(ohm.m.)$

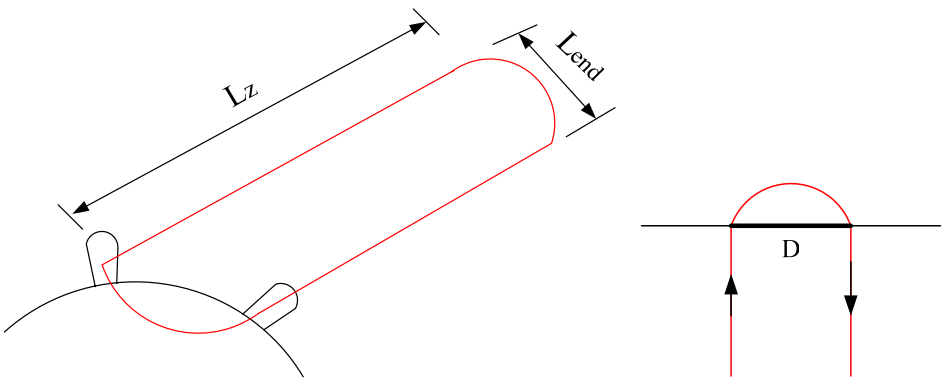

FIGURE 3-15 Show the copper wire per turn

$$D = \tau_p = \frac{2\pi R_a}{2p} \qquad ; \ \tau_p : \text{pole pitch} \qquad \text{Eq. 3-5}$$

$$L_{end} = \frac{\pi D}{2} \qquad \text{Eq. 3-6}$$

$$= \frac{\pi \cdot \tau_p}{2}$$

$$= \frac{\pi}{2} \cdot \frac{2\pi\left(R_a + h_{enc}/2\right)}{2p}$$

R_a : inner stator radius = 45 mm.

h_{enc} : height of stator ≈ 9.6 mm.

so we compute

$$\tau_p = \frac{2\pi \times (45mm. + 4.8mm.)}{2 \times 2} \qquad = 78.22\ mm.$$

$$L_{end} = \frac{\pi \times 78.22mm}{2}. \qquad = 122.87\ mm.$$

but the wire goes and returns then

$$L_{end} = 2\left(L_z + L_{end}\right)$$

$$= 2(51.4\ mm. + 122.87\ mm.) \qquad = 348.55\ mm.$$

The length of the copper per turn is 348.55 *mm*. If we define N_{turn}/coil = 74 turns we can compute the total length of the copper per phase

$$L_{end\ total} = 348.55mm \times 6 \times 74 \qquad = 154.75\ m.$$

From the copper wire

$$S = \pi r^2 \qquad \text{Eq. 3-7}$$

which diameter of it is $0.55mm.$ so

$$r = \frac{D}{2} = 0.275mm. \qquad \text{Eq. 3-8}$$

$$S = \pi \times (0.275)^2 \qquad = 0.23\,mm^2$$

so

$$R_s = 1.68 \times 10^{-8}(Ohm \cdot m) \times \frac{154.75\,m.}{0.23\,mm.^2} \qquad = 10.9\ \Omega$$

The copper losses in the stator is

$$P_j = 3R_s I^2 \qquad = 3\times 10.94\times (1.5)^2 \qquad = 73.86\ W$$

3.3.5 Computation the iron losses

Core loss or iron loss is a form of energy loss which happens in electrical transformers and other inductors. Two types of iron loss are hysteresis loss and eddy current loss. The hysteresis is well known in ferromagnetic materials which the relationship between magnetic filed strength(H) and magnetic flux density(B). The hysteresis loss results from the friction between the magnetic domain. Eddy current loss occurs when the rotating magnetic field induces alternating current, called eddy current, in the iron core. The eddy current loss can be minimized by making the core with thin sheets or laminate sheets of magnetic material [7].

The iron losses can be determined by

$$P_{iron} \approx K \times f^{\alpha} \times |B|^{\beta} \times Volume\ or\ mass \qquad \text{Eq. 3-9}$$

or

$$P_{iron} = \left(A_1 \times B^2 \times f\right) + \left(C_1 \times B^2 \times f^2\right) \times mass \qquad \text{Eq. 3-10}$$

If we define

$$f = 50\,H_z$$
$$mass = 0.447\times 10^{-3} \times 8000$$
$$A_1 = 2.15\times 10^{-2}$$
$$C_1 = 6.90\times 10^{-4}$$
$$B = 1.5\ T$$

so

$$P_{iron} =$$
$$\left\{ \left[\left(2.15\times 10^{-2}\right) \times (1.5)^2 \times 50 \right] + \left[\left(6.90\times 10^{-4}\right) \times (1.5)^2 \times (50)^2 \right] \right\} \times 0.447\times 10^{-3} \times 8000$$
$$= 22.528\ W.$$

We will consider the iron losses at the stator

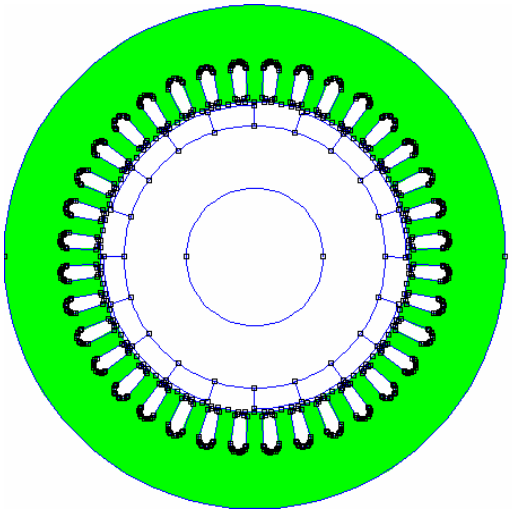

FIGURE 3-16 The picture of stator

3.3.6 Computation self-inductance and Mutual

3.3.6.1 Self-inductance

The basic of self-inductance topic needs to consider a loop of current *I* as shown in the Figure 3-17. The flux φ_1 that passes through the area S_1 bounded by the loop is [8]

$$\varphi_1 = \int_{S_1} \mathrm{B} \cdot dS \qquad \text{Eq. 3-11}$$

Suppose we pass the same current *I* through two loops, wrapped very close together, as indicated in Figure 3-17b. Each loop generates φ_1 of flux, and since they are so closely spaced, the total flux through each loop is $\varphi_{tot} = 2\varphi_1$. How much flux passes through the total area bounded by the loops, $2S_1$? Because φ_{tot} passes through the surface of each loop, the answer is $2\varphi_{tot}$, or $4\varphi_1$. We say that the two loops of current are linked by the total flux φ_{tot}.

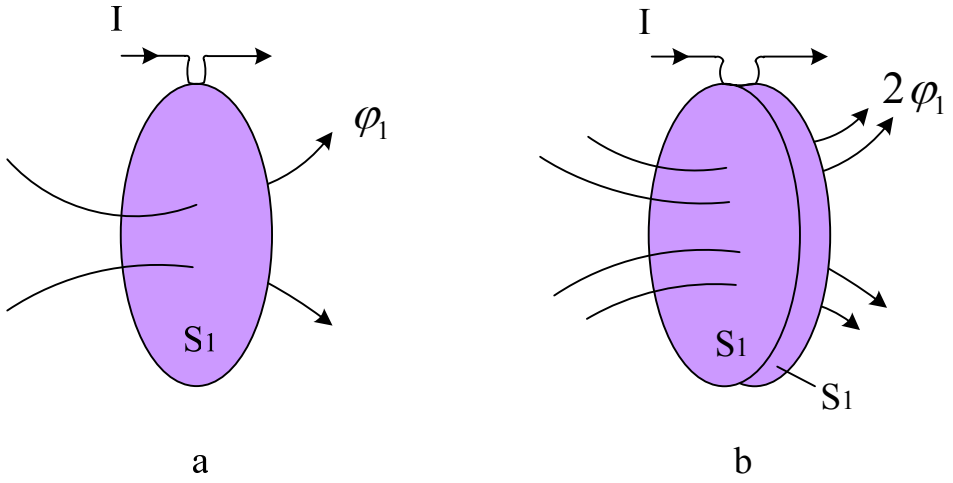

FIGURE 3-17 Loop of current. a) A single loop of current b) Two loops of current

We define the flux linkage λ as the total flux passing through the surface bounded by the contour of the circuit carrying the current. Figure 3-17a, λ is simply φ_1, and for Figure 3-17b, λ is $4\varphi_1$. For a tightly wrapped solenoid, the flux linkage is the number of loops multiplied by the total flux linking them. If we have a tightly wrapped solenoid with *N* turns,

$$\lambda = N\varphi_{tot} = N^2\varphi_1 \qquad \text{Eq. 3-12}$$

where again φ_1 is the flux generated by a single loop
N is the number of turn
λ is the flux linkage
φ_{tot} is the total flux

Now we define inductance L as the ratio of the flux linkage to the current I generating the flux,

$$L = \frac{\lambda}{I} = \frac{N\varphi_{tot}}{I} \qquad \text{Eq. 3-13}$$

This has the units of henrys (H), equal to a weber per ampere. Inductors are devices used to store energy in the magnetic field, analogous to the storage of energy in the electric field by capacitors. Inductors most generally consist of loops of wire, often wrapped around a ferrite or ferromagnetic core, and their value of inductance is a function only of the physical configuration of the conductor along with the permeability of the material through which the flux passes.

A procedure for finding the inductance is as follows:

1. Assume a current I in the conductor.
2. Determine B using the law of Biot-Savart, or Ampere's circuital law if there is sufficient symmetry.
3. Calculate the total flux φ_{tot} linking all the loops.
4. Multiply the total flux by the number of loops to get the flux linkage: $\lambda = N\varphi_{tot}$.
5. Divide λ by I to get the inductance: $L = \lambda / I$. The assumed current will divide out.

3.3.6.2 Mutual inductance

Consider the pair of coils shown in Figure 3-18. We'll let circuit 1, with N_1 loops, be our driving coil and circuit 2, with N_2 loops, be our receiving coil. When current I_1 is pushed through circuit 1, it produces flux, some of which links the N_2 loops of circuit 2. This flux is common, or mutual, to both circuits. We'll call this flux φ_{12}, where the subscripts indicate that this is the flux from B_1 of circuit 1 that link circuit 2. We find φ_{12} by integrating the dot product of B_1 and the area of a loop in circuit 2:

$$\varphi_{12} = \int B_1 \cdot dS_2 \qquad \text{Eq. 3-14}$$

The flux linkage λ_{12} is then the number of times φ_{12} links with circuit 2, or

$$\lambda_{12} = N_2\varphi_{12} \qquad \text{Eq. 3-15}$$

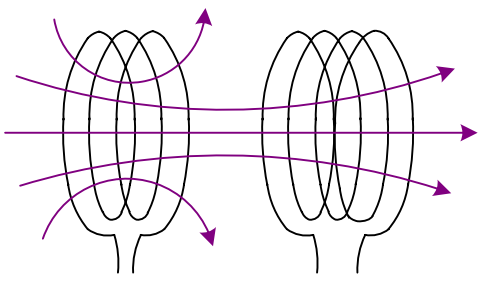

FIGURE 3-18 Pair of coils used to illustrate mutual inductance

Finally, the mutual inductance M_{12} is

$$M_{12} = \frac{\lambda_{12}}{I_1} = \frac{N_2}{I_1} \int \mathrm{B}_1 \cdot dS_2 \qquad \text{Eq. 3-16}$$

We define τ_d : slot pitch, τ_p : pole pitch [9]

$$\tau_d = \frac{2\pi R_a}{\mathrm{N}_s} = \frac{2\pi \cdot 45}{36} = 7.85 \times 10^{-3}\,\mathrm{m}. \qquad \text{Eq. 3-17}$$

$$\tau_p = \frac{2\pi R_a}{2p} = \frac{2\pi \cdot 45}{2 \cdot 2} = 70.68 \times 10^{-3}\,\mathrm{m}. \qquad \text{Eq. 3-18}$$

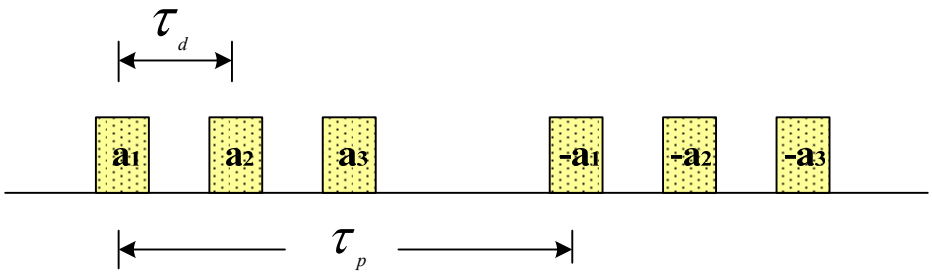

FIGURE 3-19 Showing phase (a) per one pole

$$L = \frac{\varphi}{\mathrm{I}} = \frac{\mu_0 \mathrm{N}^2 \tau_p L_z}{2e} \qquad ; e = \text{height of the magnet + the air-gap} \qquad \text{Eq. 3-19}$$

$$; \mu_0 = \text{permeability of free space}$$

$$L = \frac{\left(4\pi \times 10^{-7}\right) \times (74)^2 \times \left(70.68 \times 10^{-3}\right) \times \left(51 \times 10^{-3}\right)}{2 \times \left(7 \times 10^{-3}\right)} = 1.77\ mH.$$

$$; L = \text{self-inductance}$$

$$M_{12} = \frac{\mu_o \mathrm{N}^2 L_z \left(\tau_p - \tau_d\right)}{2e} = \frac{\left(4\pi \times 10^{-7}\right) \times (74)^2 \times \left(51 \times 10^{-3}\right) \times \left(70.68 \times 10^{-3} - 7.85 \times 10^{-3}\right)}{2 \times \left(7 \times 10^{-3}\right)}$$

$$= 1.57\ mH. \qquad ; M = \text{mutual}$$

$$M_{13} = \frac{\mu_o \mathrm{N}^2 L_z \left(\tau_p - 2\tau_d\right)}{2e} = 1.37\ mH.$$

Inductance Matrix

$$\begin{bmatrix} L_{11} & L_{12} & L_{13} \\ L_{21} & L_{22} & L_{23} \\ L_{31} & L_{32} & L_{33} \end{bmatrix} = \begin{bmatrix} 1.77 & 1.57 & 1.37 \\ 1.57 & 1.77 & 1.57 \\ 1.37 & 1.57 & 1.77 \end{bmatrix}$$

$$\varphi_1 = L_1 i_1 + \mathrm{M}_{12} i_2 + \mathrm{M}_{13} i_3 \qquad \text{Eq. 3-20}$$

$$\varphi_2 = L_2 i_2 + \mathrm{M}_{21} i_1 + \mathrm{M}_{23} i_3 \qquad \text{Eq. 3-21}$$

$$\varphi_3 = L_3 i_3 + \mathrm{M}_{32} i_2 + \mathrm{M}_{31} i_1 \qquad \text{Eq. 3-22}$$

$$\varphi_t = \varphi_1 + \varphi_2 + \varphi_3 \qquad \text{Eq. 3-23}$$

$$= (L_1 + L_2 + L_3 + 4L_{12} + 2L_{13}) i$$

$$; \; L_{e\varphi} = (L_1 + L_2 + L_3 + 4L_{12} + 2L_{13})$$

$$= 3(1.77) + 4(1.57) + 2(1.37) \qquad = 14.33 \; mH.$$

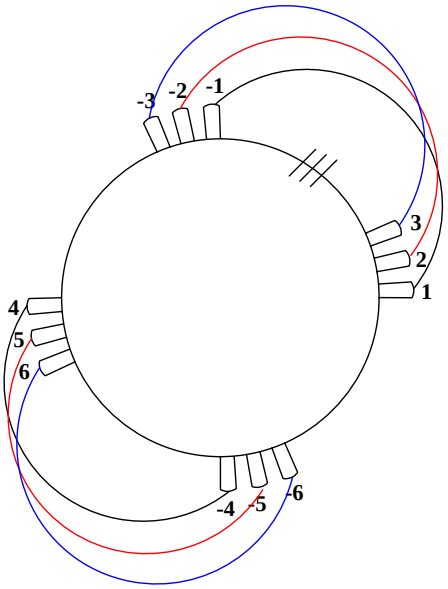

FIGURE 3-20 The winding of phase a

Inductance at phase a $= 2 \times L_{e\varphi} = 28.66 \; m\mathrm{H}.$

if we have two slots

FIGURE 3-21 Showing of two slots

$$\begin{bmatrix} \varphi_1 \\ \varphi_2 \end{bmatrix} = \begin{bmatrix} L_{11} & M_{12} \\ M_{21} & L_{22} \end{bmatrix} \begin{bmatrix} i_1 \\ i_2 \end{bmatrix}$$

$$\varphi_1 = L_{11} i_1 + M_{12} i_2 \qquad \text{Eq. 3-24}$$

$$\varphi_2 = L_{22} i_2 + M_{12} i_1 \qquad \text{Eq. 3-25}$$

the winding is in series then $i_1 = i_2$

$$\begin{aligned} \varphi_t &= \varphi_1 + \varphi_2 \qquad \text{Eq. 3-26} \\ &= \left(L_{11} + L_{22} + 2M_{12}\right) i_1 \\ &= L_{e\varphi} \times i \end{aligned}$$

3.3.7 Computation the permanent magnet

In order to design the thickness of magnet, we compute the magnetic air-gap and use the specification from geometry of the motor and then we choose:
the air gap = 0.5 mm. + 1 mm.
so, the magnetic air-gap = 1.5 mm. = e

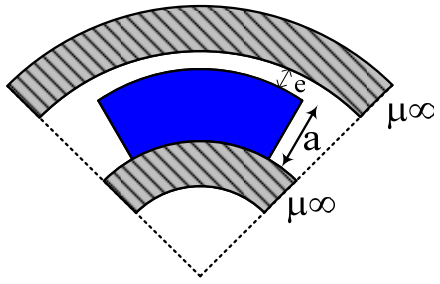

FIGURE 3-22 The feature of air-gap and permanent magnet thickness of the rotor

and we choose B_e = 0.8 T

Magnets : B_r = 1 T (Material of NdFeB)

$$B_e = B_r \frac{a}{a+e} \qquad \text{; a - height of the magnet} \qquad \text{Eq. 3-27}$$

$$a = e \times \frac{B_e / B_r}{1 - B_e / B_r}$$

so,

$$a = 1.5\ mm. * \frac{0.8}{1-0.8} = 6\ mm.$$

$$R_r = R_a - \text{e} - a = 37.5\ mm.$$

; R_r is the radial of the rotor
; R_a is the internal diameter of stator
; a is the thickness of magnet

The detail of any part is depicted in Figure 3-23.

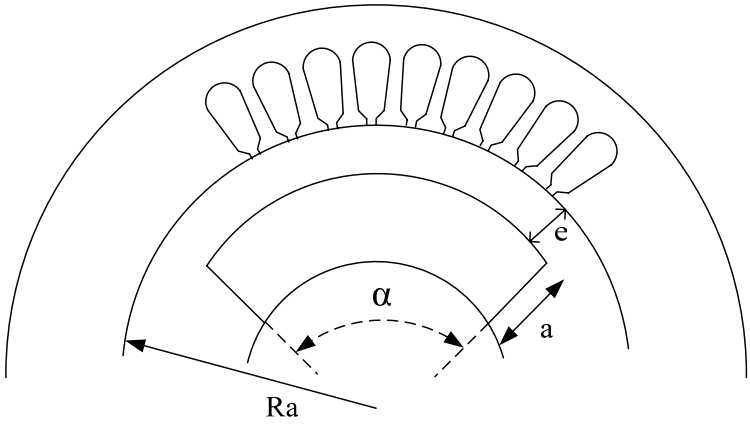

FIGURE 3-23 Magnet span of the rotor

where α is the magnet angle or called magnet span.

Mechanical teeth pitch is

$$\frac{360°}{36} = 10° \quad ; 36 \text{ are the number of slot.}$$

Electrical teeth pitch is p time mechanical teeth pitch, so

$$\tau_{d-elec} = p \times 10 = 2 \times 10 = 20° \quad ; p \text{ is the number of pole.}$$

We can not find the shape of the magnet in one piece per pole, so we will use many rectangular permanent magnets. Figure 3-24 shows the feature to design the permanent magnet. From the simulation the optimum angle is $72° = (4/5) \times 90°$, as we will see in the chapter 4. So, if we divide the magnet into 4 blocks, the span of each block is $\frac{72}{4} = 18$ deg.

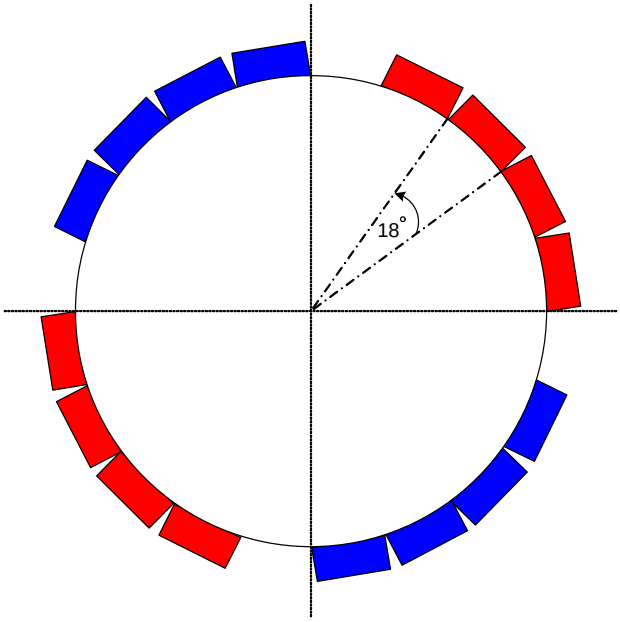

FIGURE 3-24 The feature to design the permanent magnet

Figure 3-25 shows one piece of the permanent magnet.

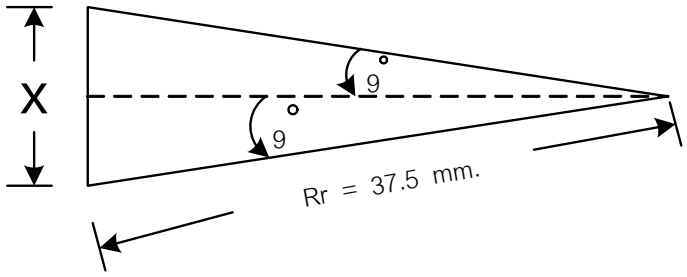

FIGURE 3-25 Piece of the permanent magnet

From the specification of machine if we consider in one pole we have

$$\frac{90°}{5} = 18°$$

we use 4 pieces of the permanent magnet, then

$$18°\times 4 = 72°$$

This calculated result is the optimum angle which corresponds to the previous result.

$$\tan(9°) = \frac{x}{2\times R_r}$$

$$x = 2\times R_r \tan(9°) = 11.87\,mm.$$

But the dimension of the magnet from the manufactory do not have the calculated value, so we will choose the nearest value and change the value of x then we define

$$x = 12\ mm.$$

$$12\,mm. = 2\times R_r \tan(9°)$$

$$R_r = 37.88mm. \cong 38\,mm.$$

so the length x is

$$x = 2 \times R_r \tan(9°)$$

$$= 12.037\ mm.$$

when R_r had changed , so the air-gap will change too and yield

the air-gap from $1.5\,mm. \Rightarrow 1\,mm.$ (because $R_r = 37.5mm. \Rightarrow 38mm.$)

Figure 3-26 shows the dimension of the permanent magnet per one piece.

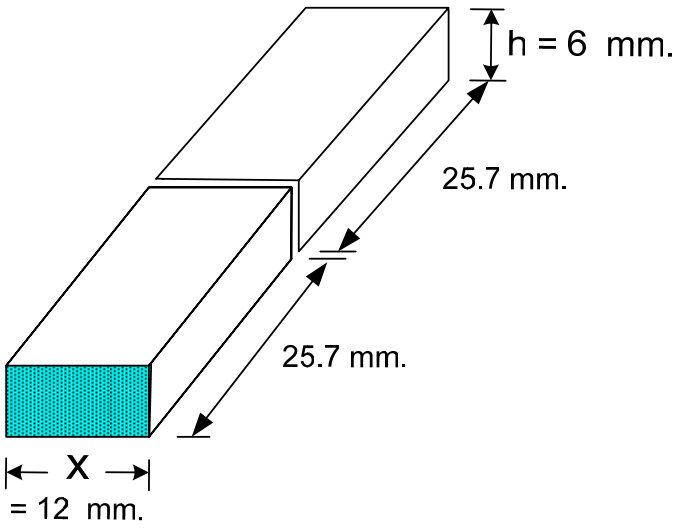

FIGURE 3-26 Dimension of the permanent magnet per one piece

Therefore, the require number of permanent magnets is

$$= (4 \times 2) \times 4 \qquad = 32 \ pcs.$$

3.3.8 Torque and cogging torque

3.3.8.1 Torque

The torque obtained from the FE analysis were plotted as a function of the position. Maxwell's stress method can be used in computing the torque. Maxwell stress tensor is one of the most used methods, because of its simplicity but is not appropriate very well for small air-gaps because it induces numerical errors. Indeed, its precision strongly depends on the method of discretization employed and the selected contour. To obtain correct results, it is necessary to mesh the air-gap very finely. Indeed, one considers a cylinder of the radius R, surrounding the rotor on which one calculates the torque by the expression:

$$\Gamma = RL \int BH \, ds$$

or

$$\Gamma = \sum \frac{E \times I}{\Omega} + Cogging \ Torque \qquad ; \ \Omega \Rightarrow \text{rad/sec}$$

However, the torque can also be computed by analytical formulation [9]

$$\Gamma = 4pq \cdot NI \cdot B_e L_z R_a$$

$$= 4 \times 2 \times 3 \times 74 \times 1.5 \times 0.85 \times 0.051 \times 0.045 \qquad = 5.19 \ N.m.$$

where p : number of pole pair

q : number of stator per pole and phase

N : number of turn

I : the current in V_{rms}

B_e : the magnetic flux in the air-gap

L_z : stack length

R_a : internal radius of stator

3.3.8.2 Cogging torque

Cogging torque arises from the interaction between permanent magnets (PMs) and slotted iron structure and manifests itself in almost all types of PM motors in which the air-gap is not constant. Under dynamic conditions, the pulsating cogging torque, of zero net value, can be transmitted via the rotor to the load, causing difficulty in position and speed control, and through the stator frame, inducing vibrations, acoustic noise and possible structural resonances. In particular, the cogging torque in high precision spindle systems is to be minimized at any cost.

Analytical calculation of cogging torque has been found using flux density function and air-gap permeance function. In a well designed motor the torque ripple and cogging should both be negligible, but it is possible for the torque ripple to exceed the cogging torque by a large amount if the motor has an inappropriate combination of winding layout, drive current and internal geometry. Manual rotation of a disconnected motor gives no indication whatever about torque ripple.

A summary of methods for reducing cogging torque is given by [10] :

1. Increase air-gap length
2. Use fractional slots/pole
3. Use larger number of slots/pole
4. Use thick tooth tips to prevent saturation
5. Keep slot openings to a minimum
6. Use magnetic slot-wedges
7. Skew stator stack or magnets
8. Radius or chamfer magnet poles
9. Radius or chamfer stator tooth tips, or punch holes in tooth tips
10. Vary the magnetization of the magnet poles
11. Use bifurcated teeth
12. Use lower magnet flux-density
13. Compensate cogging by modulating drive current waveform

3.4 Rotor design

When a rotor is placed in the opening of a stator, supported by bearings, and the appropriate alternating currents are supplied to the windings, the rotor will turn like an AC motor. See the structure of such a motor in Figure 3-27.

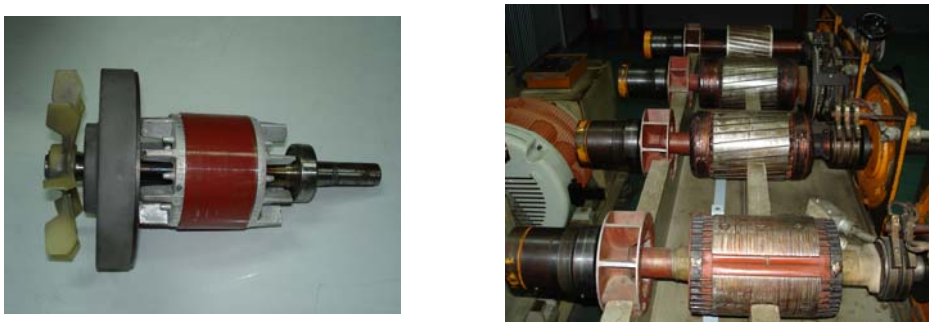

FIGURE 3-27 Typical of the rotor

Two shapes of permanent magnet are studied in this thesis:

3.4.1 Tile shape of permanent magnet

Permanent magnet have the tile shape is shown in the Figure 3-28. First step we had considered this shape which is the high efficient EMF value but finally we could not use it, owing to the size that manufactory build is not corresponding shape, so we must decide the other one it is square shape.

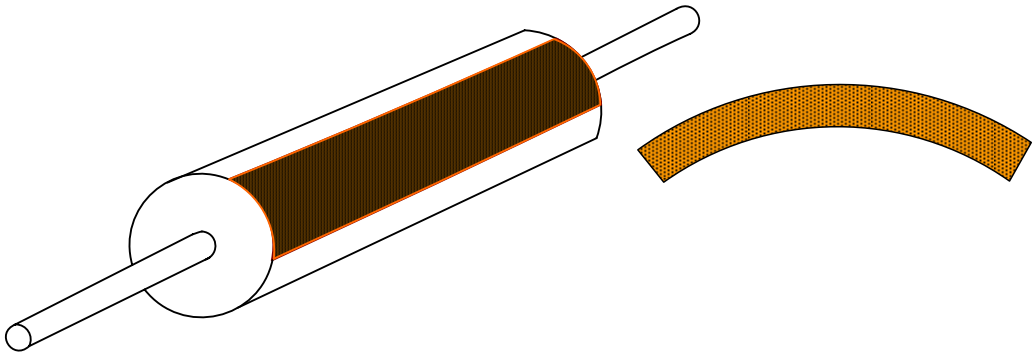

FIGURE 3-28 Tile-shape permanent magnet rotor

3.4.2 Square shape of permanent magnet

Square-shape is the new method that we have considered. Even if the values that we received were not good as same as the tile shape, but it is nearly the old one. Figure 3-29 shows square shape of permanent magnet on the rotor.

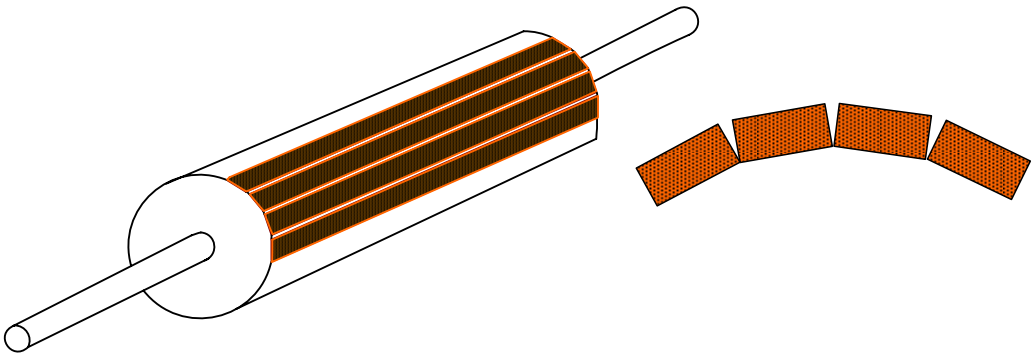

FIGURE 3-29 Square-shape permanent magnet rotor

In order to design the rotor we must use the mechanical software program called Auto CAD which is illustrated in the Figure 3-30 and we can see the model of the rotor before construct.

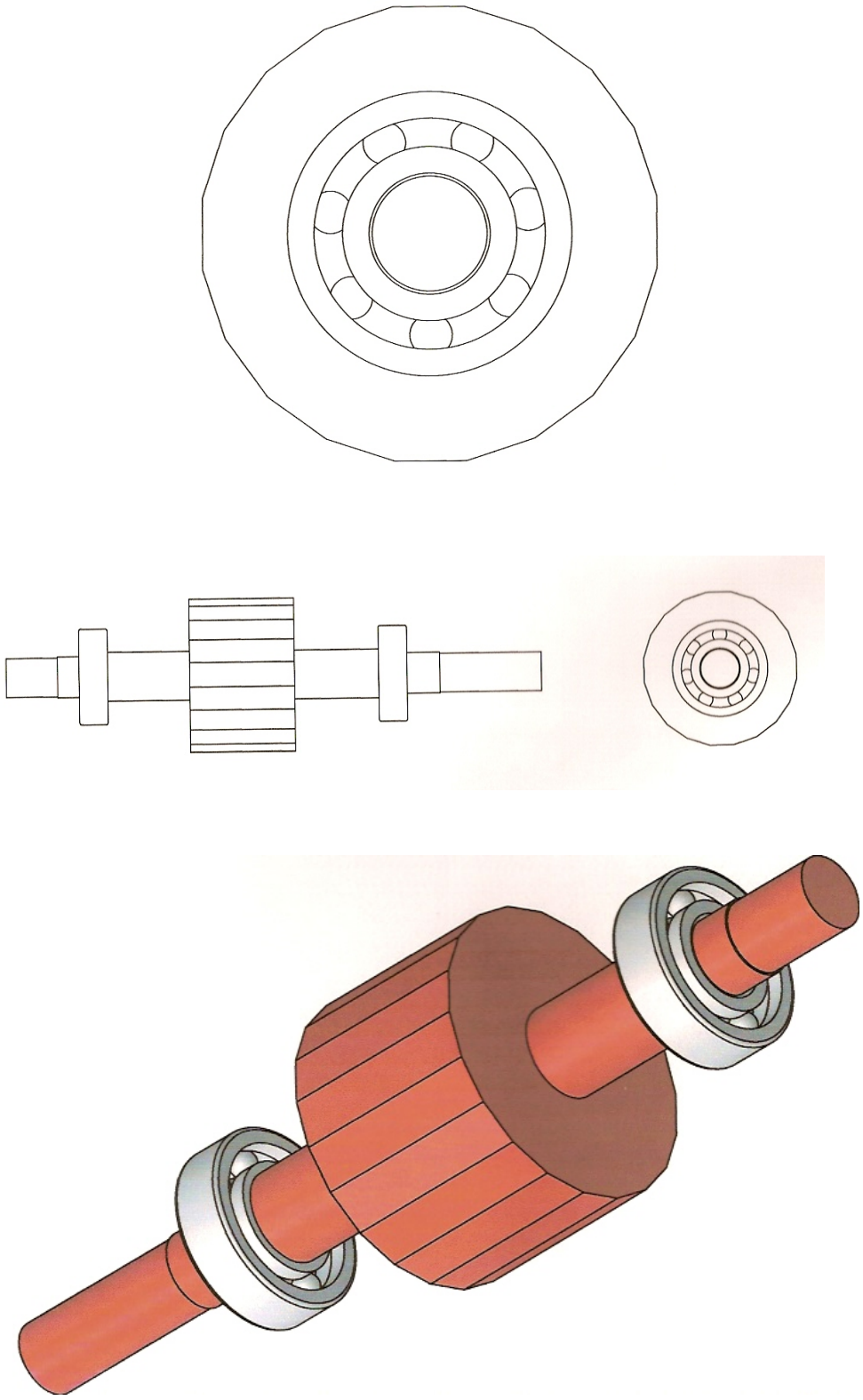

FIGURE 3-30 The dimension of the rotor using Auto CAD software

Figure 3-31 shows the structure of iron core(XC10) rotor before mounting the permanent magnets on the surface which obtains the model from the mechanical software.

FIGURE 3-31 The iron core rotor

Figure 3-32 shows of the procedure to assemble the pieces of the permanent magnet on the rotor.

FIGURE 3-32 The magnet on the iron core rotor

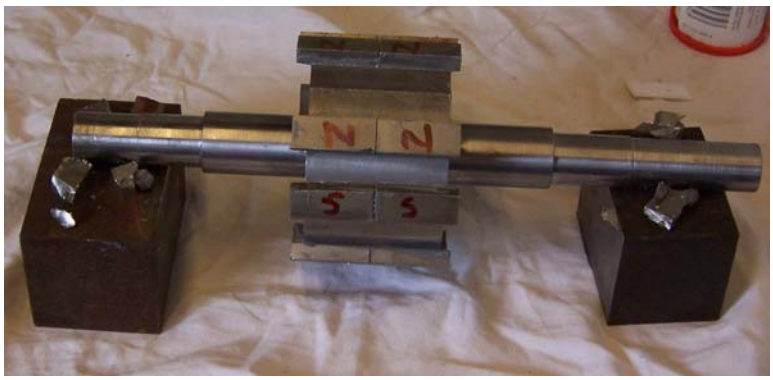

FIGURE 3-33 The magnet on the rotor

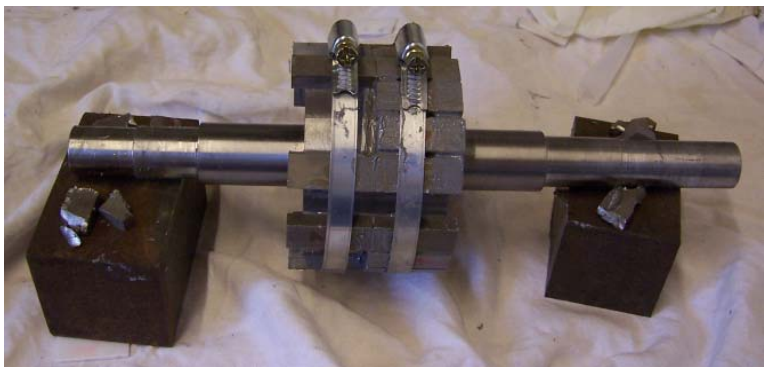

FIGURE 3-34 Gluing the magnet on the rotor

When we glue the permanent magnet we must bring it into the furnace in order to adhere the magnet with the iron core rotor. To glue the magnet is very difficult because of the magnetizing between the magnet bar and when the amount of the magnet bars are increasing the effect to glue is more difficult too. The glue is thermoduric and becomes dry with the temperature.

FIGURE 3-35 Put the rotor with the magnet into the furnace

Finally the samarium cobalt magnets have been fixed on the rotor and prepare to assemble with the stator.

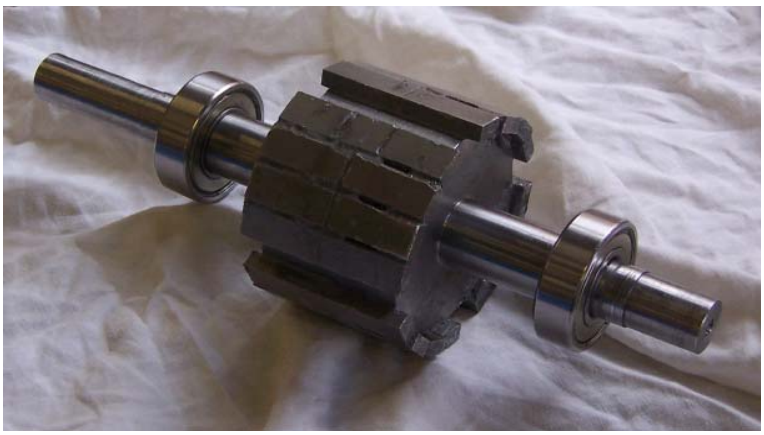

FIGURE 3-36 The iron core rotor with the permanent magnets

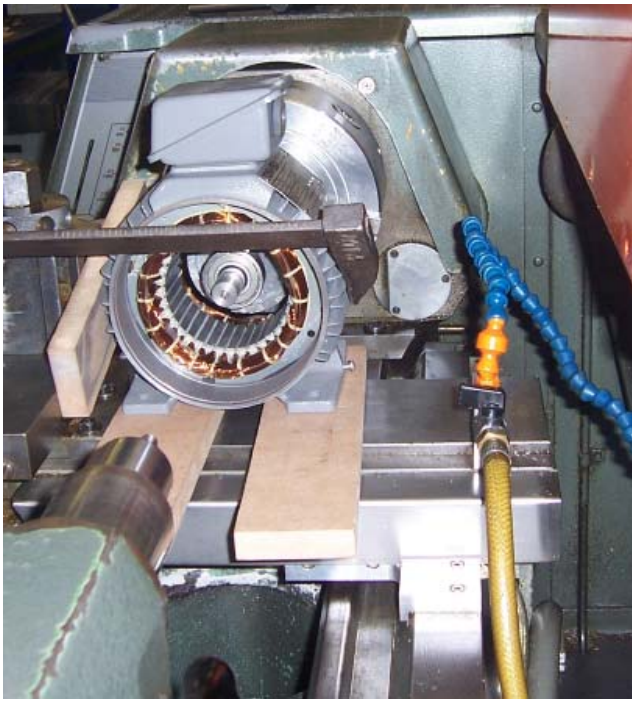

FIGURE 3-37 Assembly of the motor

3.5 Chapter summary

This chapter describes the fundamentals aspects which are used to design by the finite element method and Auto CAD software in order to construct the new rotor with samarium cobolt permanent magnet fixed on it and then we assemble the rotor to the stator.

CHAPTER 4
CALCULATION AND THE EXPERIMENTAL RESULTS

The software called Finite Element Magnetic Method (FEMM) is used in the design calculation of the PM machine. The main objective is to find the optimum magnet span of the rotor.

4.1 The calculation results

Analytical design of the motor by the finite element to compute the exactly performances is shown as the form of flux line, flux density and meshes in Figure 4-1 and Figure 4-2.

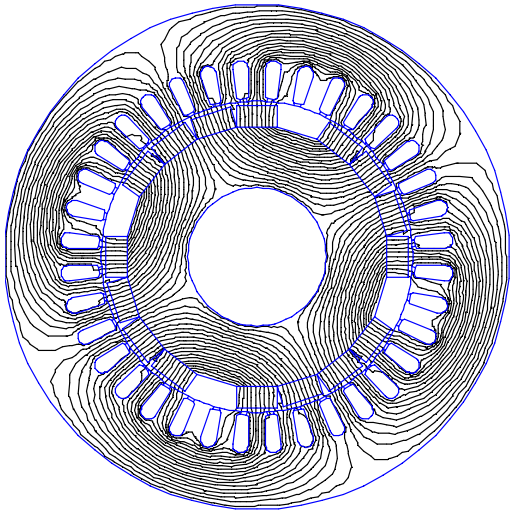

FIGURE 4-1 The flux line

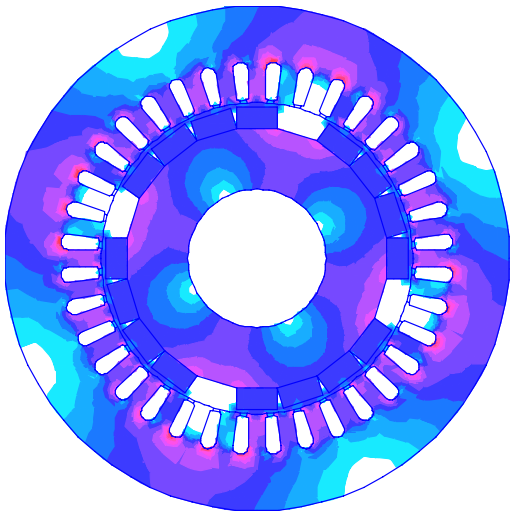

FIGURE 4-2 The flux density

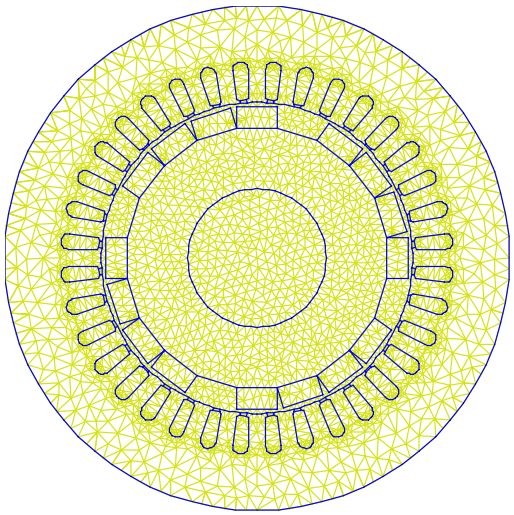

FIGURE 4-3 A view of the mesh at no load

Two shapes of the permanent magnet on the rotor are investigated as follows:

4.1.1 Tile shape permanent magnet

The tile shape of magnet gives high EMF value. But, due to the manufacturing process in producing the PM, it is rather difficult to find a suitable size of the magnet to be fitted to the rotor. So, in practice we replace them with the square shape ones.

Figure 4-4 shows each harmonic for the various values of the magnet span and the evolution of THD and modified-THD as shown in Figure 4-5 while the form of modified-THD does not consider the 3^{rd} and 9^{th} harmonics then the optimum value of magnet span is 72 degrees.

In a star-connected 3-phase motor, the current harmonics multiple of 3 are nil, therefore the emf harmonics multiple of 3 do not create the torque. That is why the 3^{rd} and 9^{th} harmonics are not considered in modified-THD.

4.1.2 Square shape permanent magnet

To solve the problem of the tile shape permanent magnet we can instead use square shape and choose the nearest dimension of the old one.

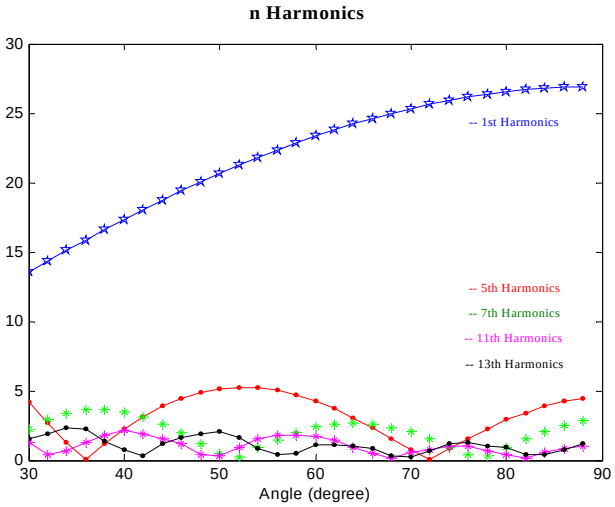

FIGURE 4-4 EMF-Percentage in each harmonic

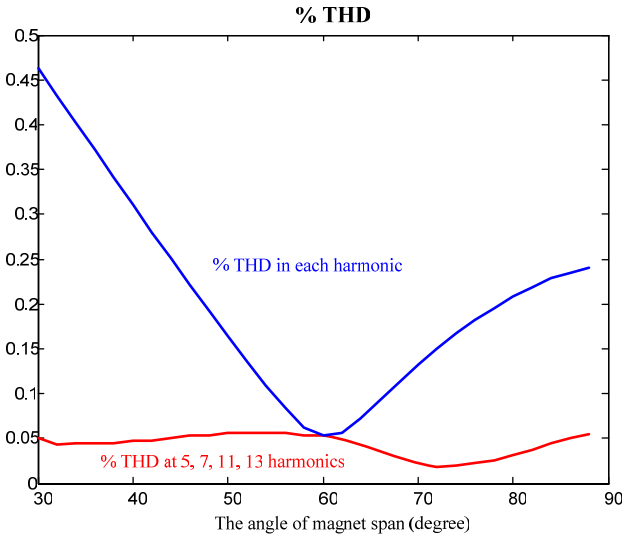

FIGURE 4-5 THD and the modified THD for different value of magnet pole span

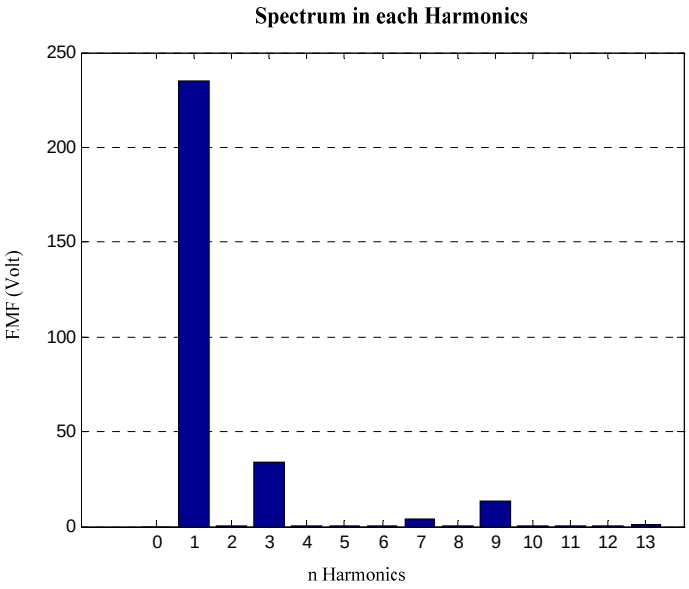

FIGURE 4-6 Spectrum in each harmonic per phase

TABLE 4-1 The EMF values in each harmonic per phase

Harmonics	EMF : Amplitude	EMF : Vrms
1	235.05	166.18
3	34.02	24.05
5	0.16	0.11
7	3.67	2.59
9	13.69	9.68
11	0.29	0.21
13	1.14	0.80

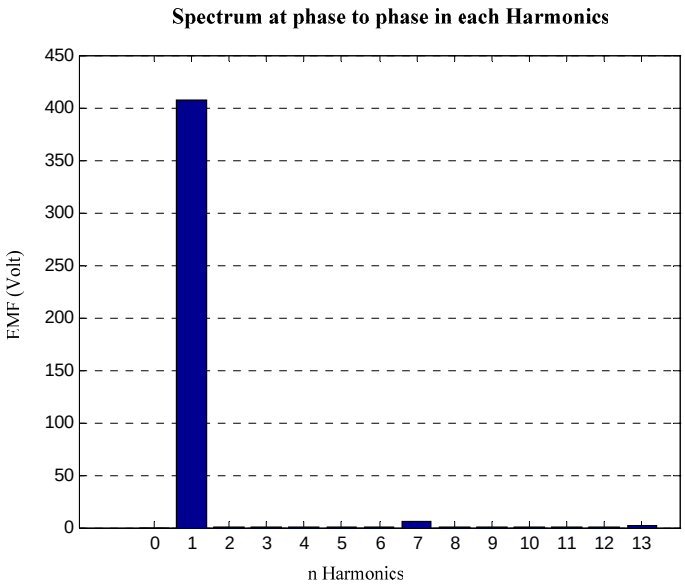

FIGURE 4-7 Spectrum in each harmonic at line to line

TABLE 4-2 The EMF values in each harmonic at line to line.

Harmonics	EMF : Amplitude	EMF : Vrms
1	407.10	287.82
3	0.02	0.02
5	0.31	0.22
7	6.37	4.50
9	0.06	0.04
11	0.55	0.39
13	2.03	1.44

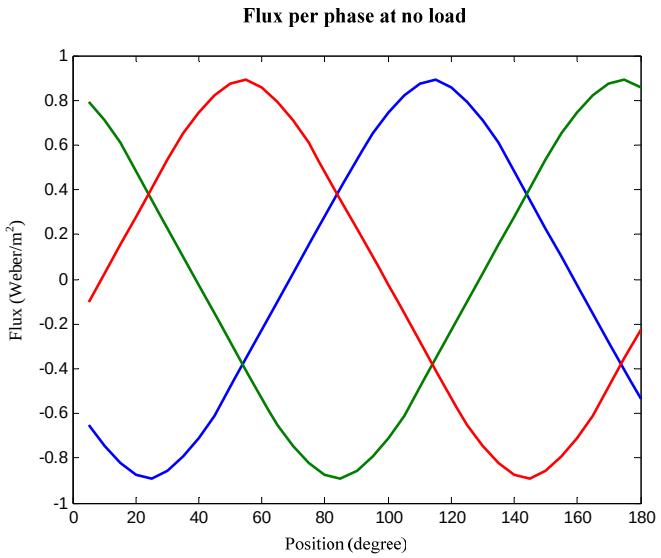

FIGURE 4-8 The flux per phase

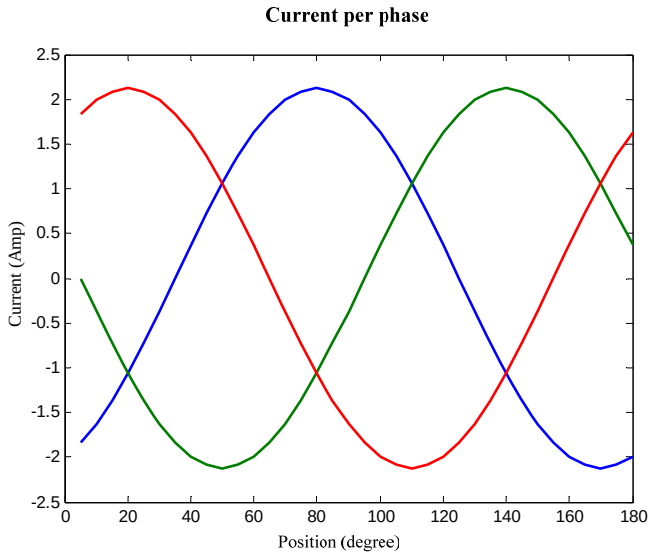

FIGURE 4-9 The current per phase

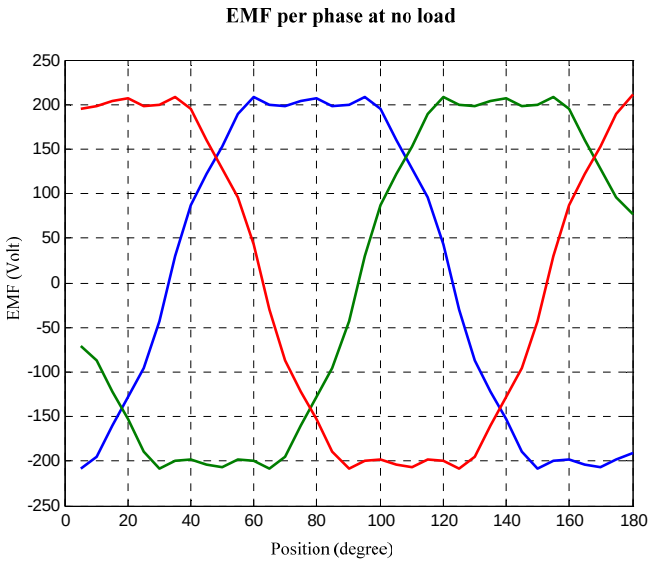

FIGURE 4-10 The back-emf per phase

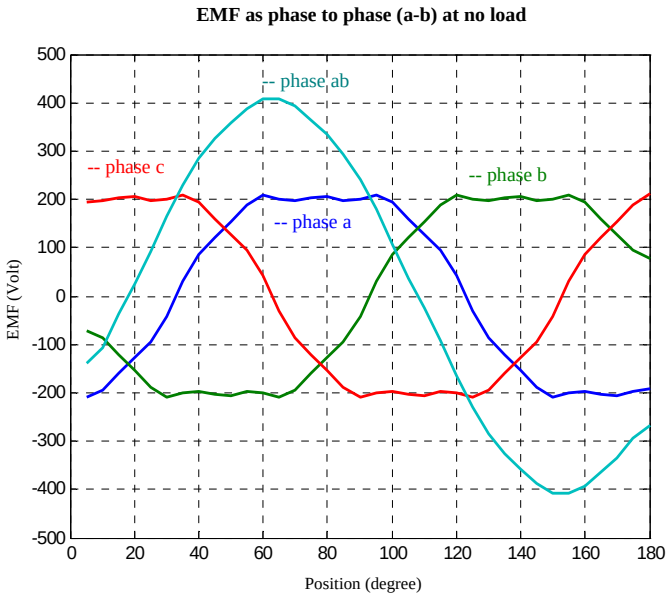

FIGURE 4-11 The back-emf per phase and line to line

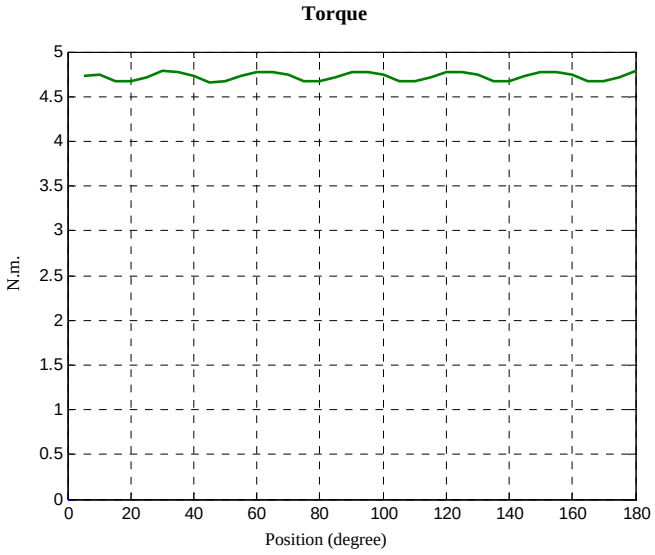

FIGURE 4-12 Torque of the motor at the current of 1.5 A.

When we used the several permanent magnet blocks or magnet segmentation, there will be the interaction between the magnets and the slot of iron structure. This action results in the so called “cogging torque” as shown in Figure 4-13.

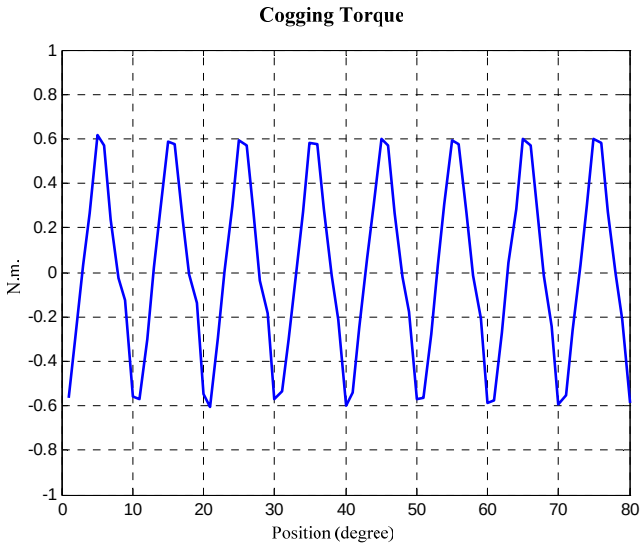

FIGURE 4-13 The cogging torque

The cogging torque obtained for this motor is about 1.2 N.m. peak to peak value which is too high. If we want to reduce this value we can act on the stator teeth geometry. In our case the stator lamination and winding are fixed. Another possibility is to act on the rotor geometry by skewing the magnet. Figure 4-14 shows the case where the rotor magnet is skewed on 3 blocks.

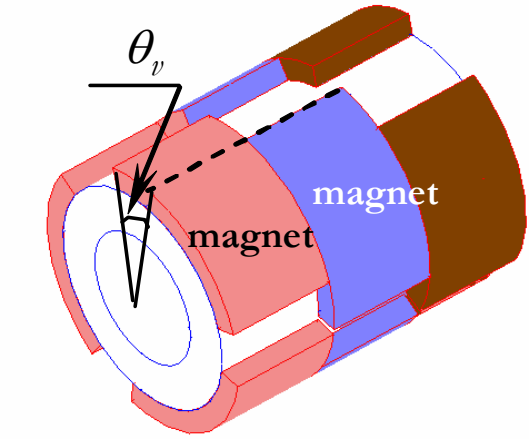

FIGURE 4-14 The case of the rotor magnet are skewed on 3 blocks

In the case of our machine, two pieces of the magnet may be used on the axial direction of the rotor. If we make a skewing of $\theta_v = \frac{\tau_d}{2} = 5°$, every axial part produces a cogging which is about 0.6 N.m. peak to peak value and shift the angle of 5°. Figure 4-15 shows the 2 waveforms of cogging torque. So the total cogging torque is the sum of these 2 cogging torque which will be of a smaller amplitude. Figure 4-16 show the total cogging torque that should be obtained if the rotor is skewed in two axial pieces. It is about 0.3 N.m. peak to peak value. But in practice we did not do this skewing because of technological difficulties. So our rotor is not skewed.

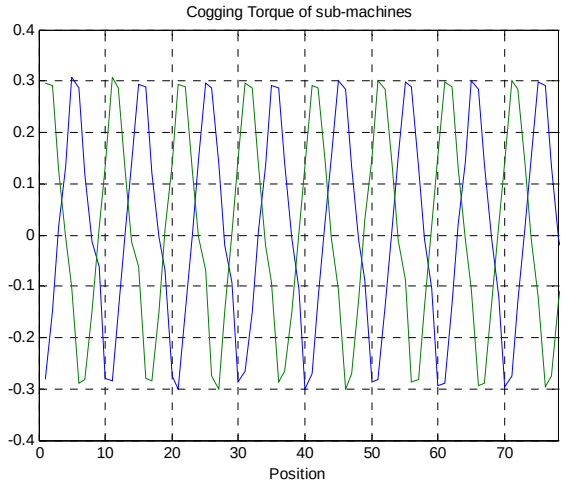

FIGURE 4-15 Two waveforms of the cogging torque

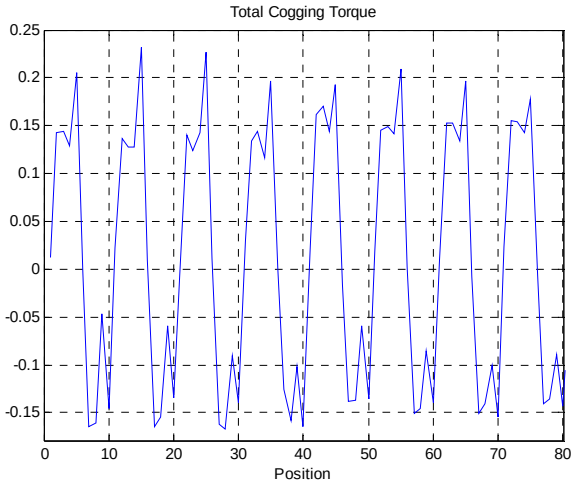

FIGURE 4-16 The cogging torque in case of the rotor is skewed in two axial pieces

4.2 The experimental results

The rotor is constructed base on the magnet span and the magnet segmentation discussed previously. The experiment is carried out by investigating the back EMF generated by the motor. This is done by operating the motor as a no-load generator at the designed speed of 1500 rpm and measuring the terminal voltages. Figure 4-17 and table 4-3 show the harmonic of the back EMF. Figure 4-18 shows the back EMF for each phase. Figure 4-19 shows the line-to-line voltages which are almost sinusoidal waveforms. It is observed from the experimental results that the waveform and the harmonic contents of the back EMF agree well with the design calculated from FEMM.

In order to verify the torque calculation, the motor was driven by a current – controlled inverter. It was brought into synchronism by slowly increasing the frequency of the inverter. Since the measurement of the instantaneous torque is not possible for the time being, the average torque is measured instead. Figures 4-20 to 4-25 show different values of average torque and the motor current. It is observed

form Figure 4-25 that at the torque of 5 N-m, the current is 1.58A which very close to the calculation result shown in Figure 4-12. Figure 4-26 shows the relationship of back EMF and the motor speed. The relationship between torque and current is shown in Figure 4-27.

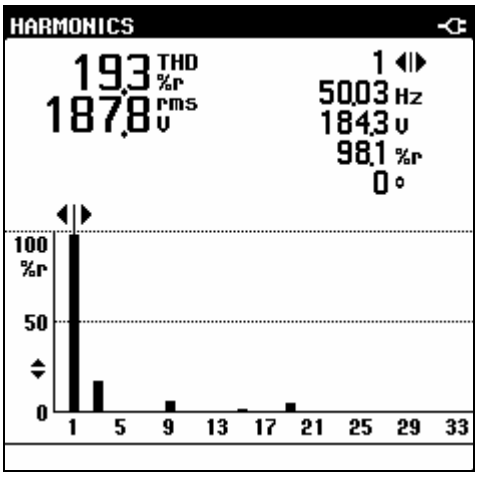

FIGURE 4-17 The spectrum of EMF

TABLE 4-3 The EMF values in each harmonic that read from the spectrum.

Harmonics (n)	EMF : Vrms (experiment)
1	184.3
3	32.6
5	2.1
7	2.1
9	11.0
11	0.3
13	1.0

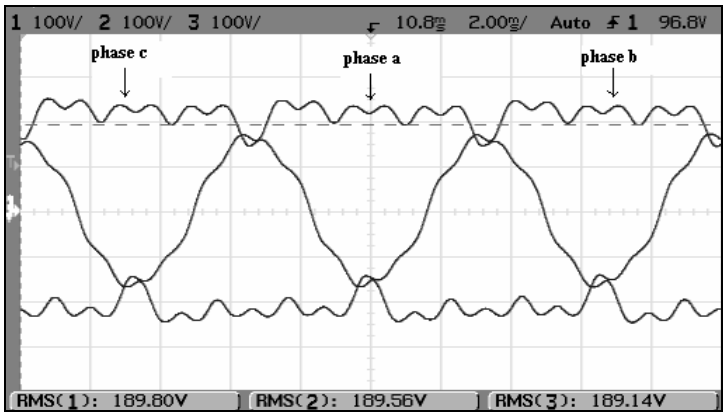

FIGURE 4-18 The EMF wave form in each phase

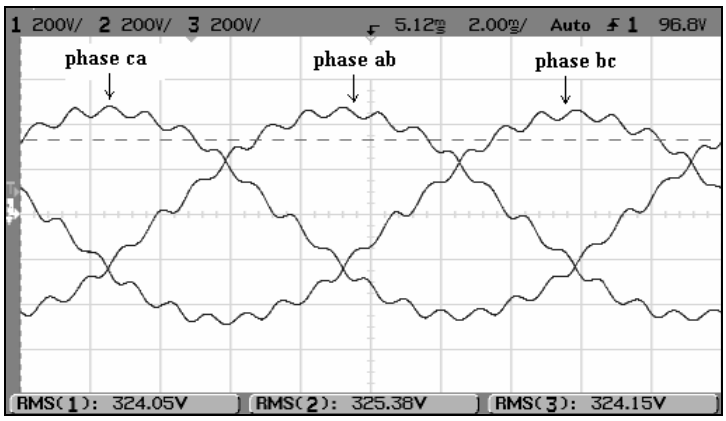

FIGURE 4-19 The EMF wave form in each line to line

TABLE 4-4 The EMF values in each harmonic per phase and line to line.

Harmonics (n)	EMF (Vrms) at phase a (experimental)	EMF (Vrms) at line to line (experimental)
1	189.5	325.3
3	32.6	0.1
5	2.1	3.3
7	2.1	3.5
9	11.0	0.1
11	0.3	0.4
13	1.0	1.7

Figure 4-20 shows the average torque.

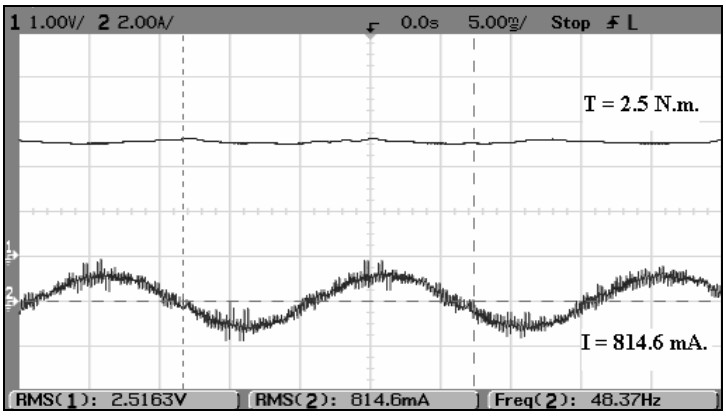

FIGURE 4-20 Load tested at 2.5 N.m.

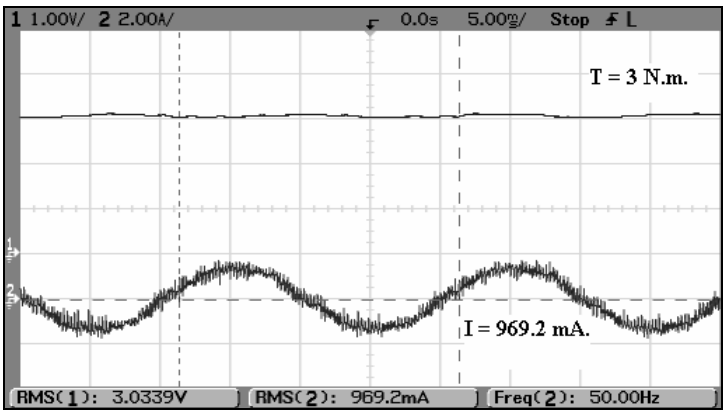

FIGURE 4-21 Load tested at 3 N.m.

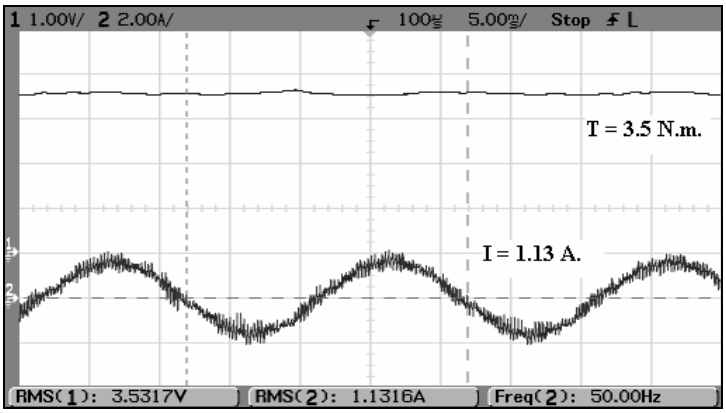

FIGURE 4-22 Load tested at 3.5 N.m.

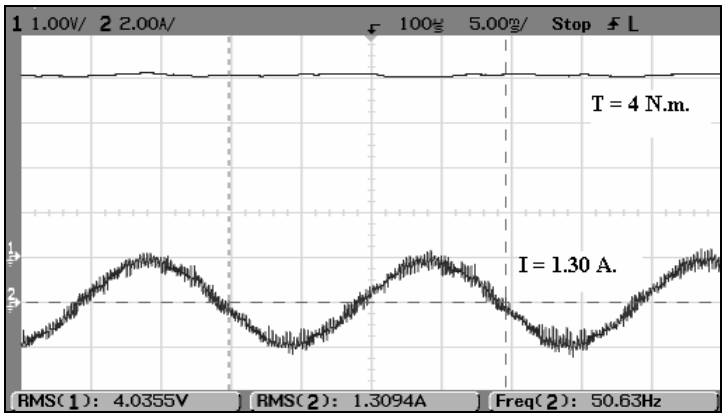

FIGURE 4-23 Load tested at 4 N.m.

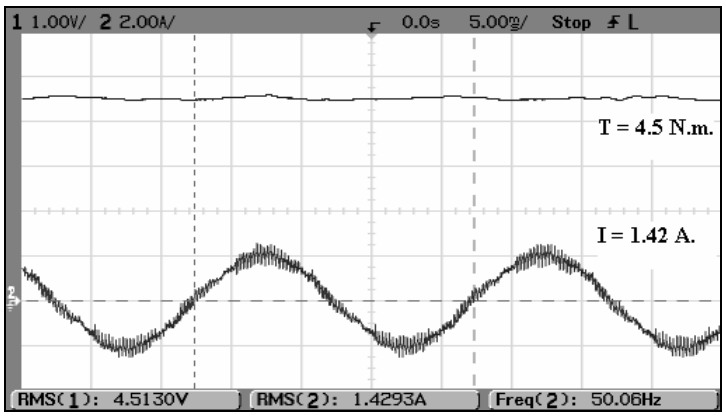

FIGURE 4-24 Load tested at 4.5 N.m.

Figure 4-25 shows the average torque at 5 N.m. and the current is 1.58 A.

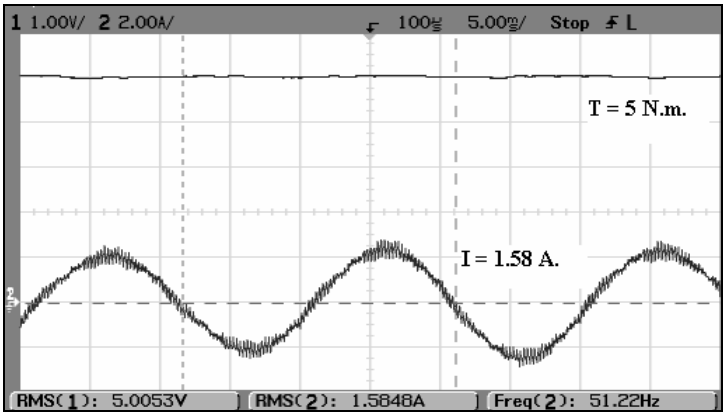

FIGURE 4-25 Load tested at 5 N.m.

The EMF value as function of speed is shown in Figure 4-26 which almost all EMF values linearize and Figure 4-27 shows the relation between the current and torque of the motor.

The relationship between the back EMF amplitude and the speed is linear when saturation of the iron is not taken into account because the magnet flux is constant.

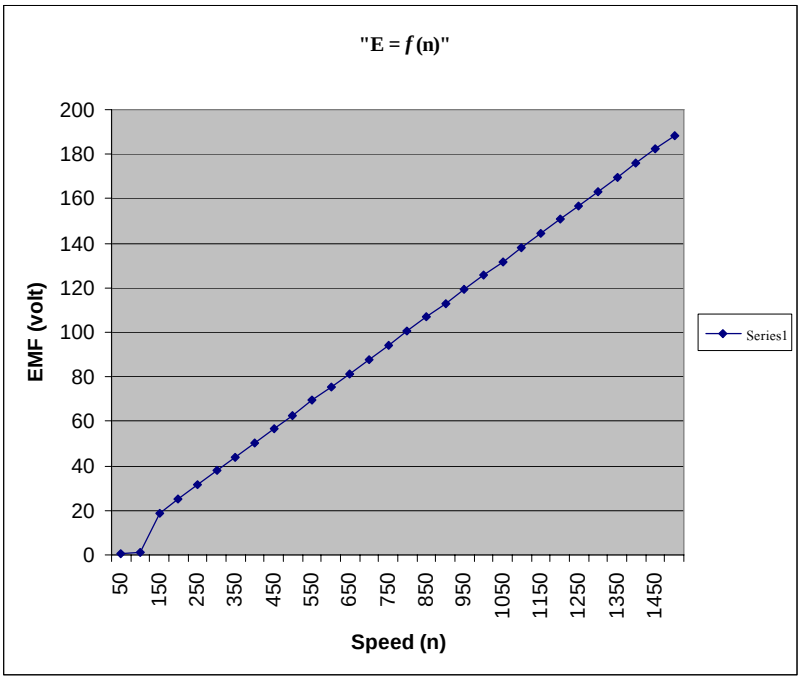

FIGURE 4-26 EMF as a function of speed.

The torque-current curve is also linear if the motor is supplied such that the angle between the current and the EMF is constant. Figure 4-27 we show this characteristic when this angle is equal to zero which corresponds to the maximum torque.

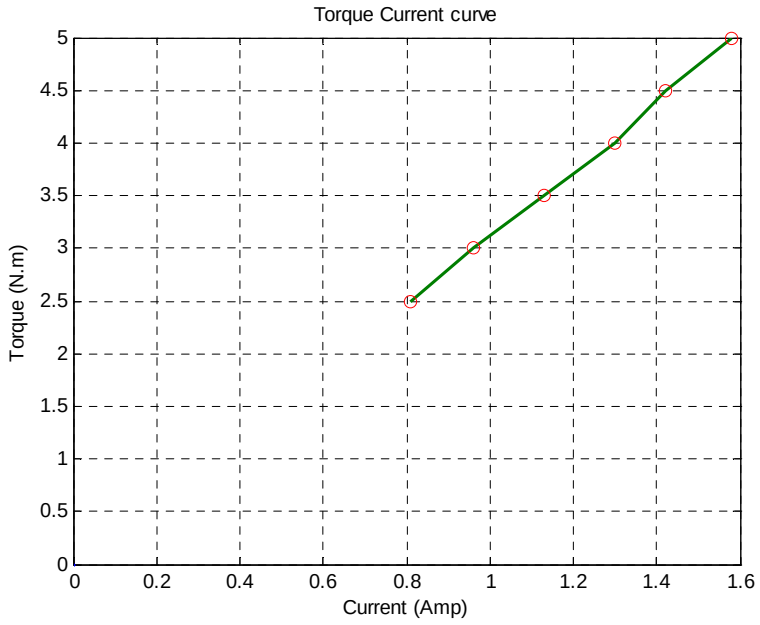

FIGURE 4-27 The relationship between the current and torque

The test bench for the experimental results is shown in Figure 4-28.

FIGURE 4-28 The test bench

4.3 Chapter summary

This chapter has explained the design of the permanent magnet rotor. The design starts by considering the tile-shape magnet, and then using the finite element analysis with FEMM to determine the optimum magnet span. The magnet span is selected to minimize the modified THD. In the construction of the rotor, several magnet blocks are used to replace the tile-shape magnet. Experimental results are in good agreement with the calculation results.

CHAPTER 5
CONCLUSIONS

Permanent magnet synchronous motors (PMSMs) have been playing an important role in high performance drive systems. However, most of the PMSMs used in the Thai industries have been imported. To reduce such import, there is the need to develop technical knowhow on the design and construction of the PMSMs. This thesis takes the first step towards this direction.

In general, the design of a PMSM involves the design of both stator and rotor. Because of technical constrains on the construction of the stator, the thesis has focused only on the design and construction of the permanent magnet rotor, while the stator structure has been taken from an existing 1-Hp induction motor without changing the winding.

The optimum magnet span is the key parameter to be determined. The finite element method using the software FEMM has been employed in the calculations. In order to achieve a sinusoidal back EMF, the magnet span has been selected to minimize the modified THD, a newly defined term representing the THD with the 3^{rd} and 9^{th} harmonics excluded. Firstly, a tile shape permanent magnet has been used in the design calculation and the optimum magnet span has been found to be 72 degrees. Then, the tile shape magnet has been replaced by several elementary SmCo magnet blocks in the construction of the rotor. Finally, the rotor has been assembled to the stator frame.

In order to verify the design calculations, the back EMF was measured when the motor was mechanically driven to operate as a no load generator. The back EMF varies linearly with the speed. At the rated speed of 1500 rpm, the line-to-line back EMFs are almost sinusoidal waveforms. However, the magnitude of the back EMF for each phase is higher than the one obtained from the calculation by FEMM. This might be due to the fact that the characteristic of SmCo magnets, iron core and stator iron used in the design may not be accurately known.

Torque has been verified by driving the motor with a current-controlled inverter. After the motor had been locked into the synchronism at the rated speed, a load torque was applied and the current was measured. The current increases linearly with the load torque. At the torque of 5 N-m, the current has been found to be 1.58 A, which is very close to the current obtained from the design calculation.

Further works need to be carried out to improve the performance of the motor. These include the design of the stator structure and the changing of the stator winding to double-layers winding with 5/6 recourse pitch.

We have studied a method to reduce the cogging torque by skewing in magnet block on the rotor. This technique should be used in the future in order to improve the quality of the torque produced by the PM machine.

REFERENCES

1. Ramdane Lateb., Noureddine Takorabet., and Farid Meibody-Tabar. "Effect of Magnet Segmentation on the Cogging Torque in Surface-Mounted Permanent Magnet Motor." IEEE Trans. Mag. 2006 : 1-4.
2. Wikipedia Foundation Inc. "Electromagnetic Field." Electrodynamics [serial online] 2006 Oct 5 [cited 2006 Oct 15].
3. N. Takorabet. MATERIALS REGIONAL WORKSHOP on Electrical Motor Design and Actuators. CODE 1A-005-00. April 26th – 30th, 2004.
4. Eckart Nipp. Permanent Magnet Motor Drives with Switched Stator Windings. TRITA-EMD-9905 ISSN-1102-0172. Royal Institute of Technology Department of Electric Power Engineering Electrical Machines and Drives. Stockholm, 1999.
5. Chen Yang. "Chen Yang SmCo Magnets Samarium Cobolt Magnets." Permanent Magnets [serial online] 2004 [cited 2006 Feb 25].
6. Pia Salminen. FRACTIONAL SLOT PERMANENT MAGNET SYNCHRONOUS MOTORS FOR LOW SPEED APPLICATIONS. Lappeenrannan teknillinen yliopisto. Lappeenranta University of Technology, 2004.
7. Wikipedia Foundation Inc. "Core loss, Eddy current, Hysteresis." Iron loss [serial online] 2006 Aug 26 [cited 2006 Oct 15].
8. STUART M. WENTWORTH. FUNDAMENTALS OF ELECTROMAGNETICS WITH ENGINEERING APPLICATIONS. 2005.
9. N. Takorabet. ACTIONNEURS ELECTRIQUES. Cours ENSEM 3ème Année Filière GE. 2005-2006.
10. J.R. HENDERSHOT JR and TJE MILLER. Design of brushless permanent-magnet motors. n.p., 1994.

APPENDIX A

The Information of Induction Motor

Specification of winding

For design and construction, this thesis focus on the permanent magnet rotor while the stator structure has been taken from an existing 1-Hp induction motor without changing the winding as depicted below.

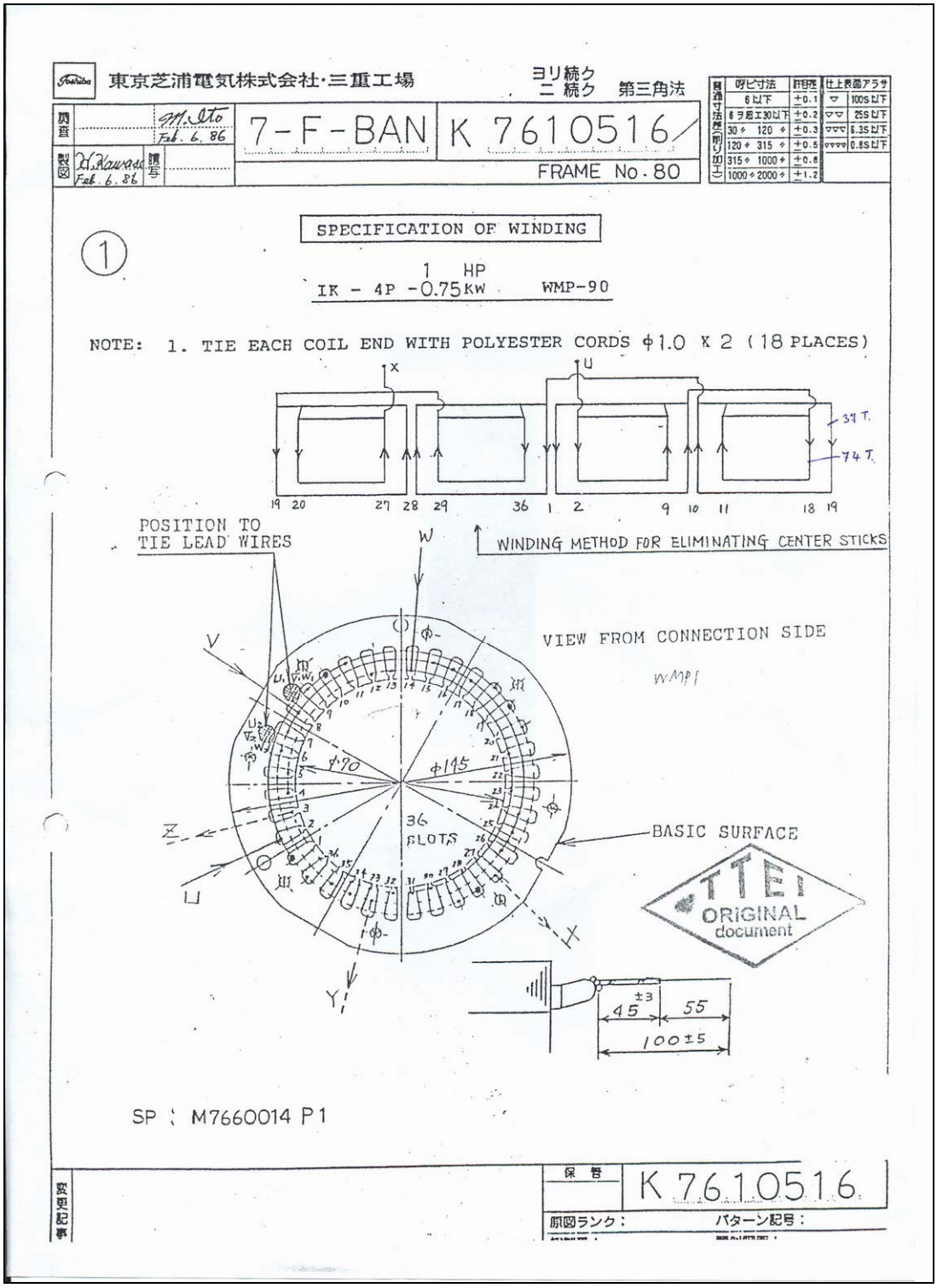

JIG and FIXTURE DRAWING

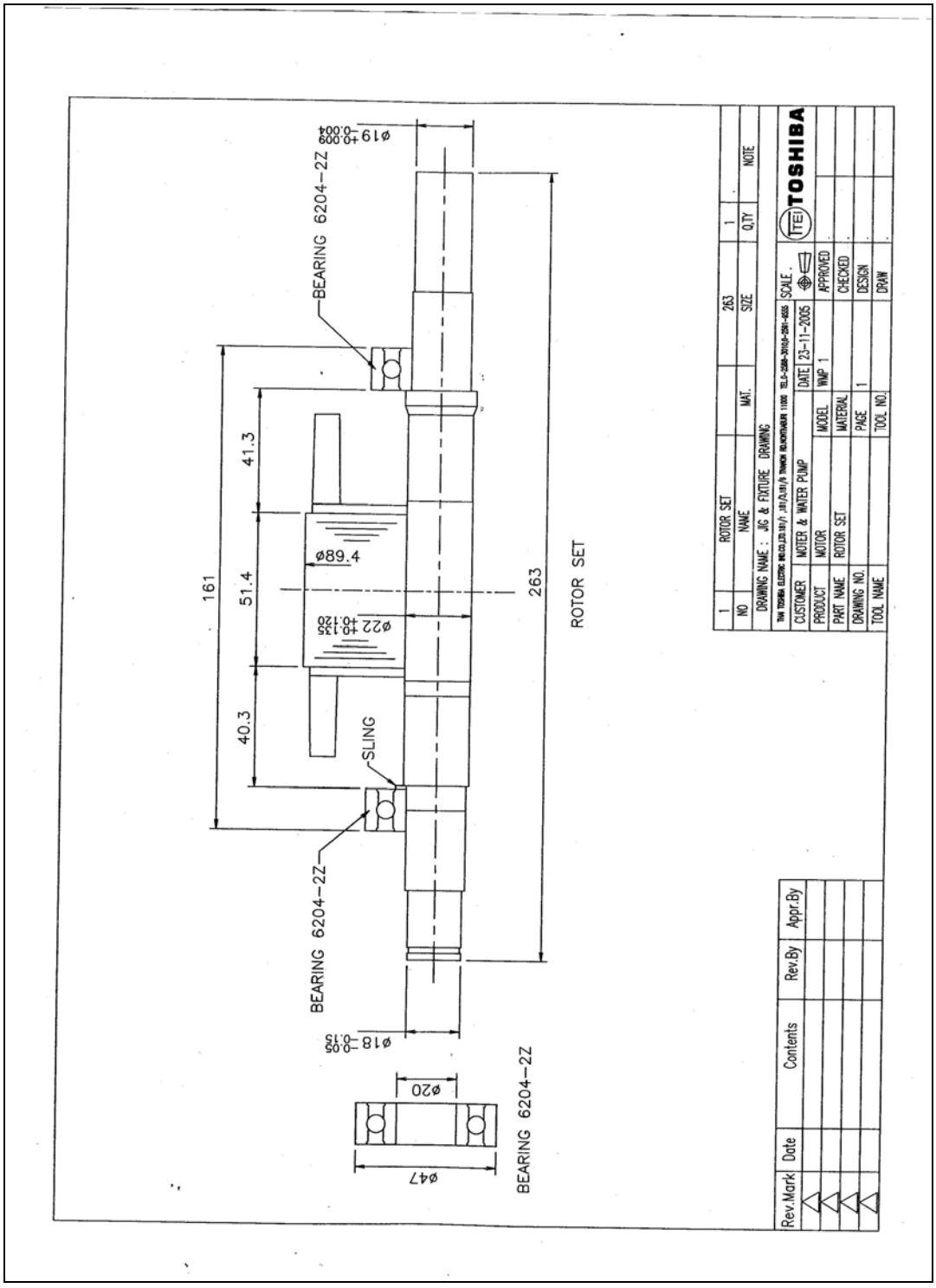

BIOGRAPHY

Name : Miss Sisuda Chaithongsuk
Thesis Title : Design and Construction of a Permanent Magnet Synchronous Motor
Major Field : Electrical Engineering

Biography

Sisuda Chaithongsuk was born in Rayong, Thailand in 1975. She received the Bachelor of Science in Technical Education Degree from King Mongkut's Institute of Technology North Bangkok(KMITNB), Thailand in 2001. As she was studying in master degree, she received the join master thesis which was the cooperation between KMITNB and INPL(France) from September 2005 – March 2006 in France.